

CHAPTER-3

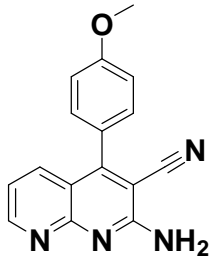
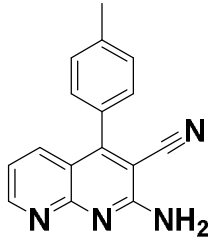
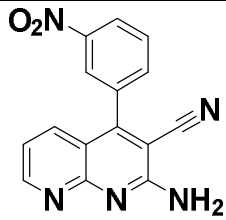
RESULTS AND DISCUSSION

3.1. Naphthyridine derivatives as Corrosion Inhibitors

Naphthyridine derivatives shows various biological activities like antibacterial, anti-inflammatory, antihypertensive and anticancer and thus widely used as drugs [Goswami *et al.* (2012)]. There are few reports on use of naphthyridine derivatives as corrosion inhibitors [Abd Elrahim and Mohamed (2014), Kalaiselvi *et al.* (2013)].

The aim of the present study was to assess the inhibition effect of three Naphthyridine derivatives namely 2-amino-4-(4-methoxyphenyl)-1,8-naphthyridine-3-carbonitrile (ANC-1), 2-amino-4-(4-methylphenyl)-1,8-naphthyridine-3-carbonitrile (ANC-2) and 2-amino-4-(3-nitrophenyl)-1,8-naphthyridine-3-carbonitrile (ANC-3) on N80 steel in 15% HCl using weight loss measurements, potentiodynamic polarization measurements, electrochemical impedance spectroscopy, quantum chemical calculations, scanning electron microscopy (SEM) and energy-dispersive X-ray spectroscopy (EDX). The molecular structure, abbreviations and IUPAC name of the synthesized compounds are given in Table 3.1.1.

Table 3.1.1 The IUPAC name, molecular structure and abbreviation of Napthyridine derivatives

| S.No. | IUPAC Name | Molecular Structure | Abbreviation |
|-------|--|--|--------------|
| 1 | 2-amino-4-(4-methoxyphenyl)-1,8-naphthyridine-3-carbonitrile |  | ANC-1 |
| 2 | 2-amino-4-(4-methylphenyl)-1,8-naphthyridine-3-carbonitrile |  | ANC-2 |
| 3 | 2-amino-4-(3-nitrophenyl)-1,8-naphthyridine-3-carbonitrile |  | ANC-3 |

3.1.1. Weight loss measurements

(i) The variation of inhibition efficiency (η %) values are tabulated in Table 3.1.2. The inspection of Table 3.1.2 reveals that inhibition efficiency increases and corrosion rate (C_R) decreases with increase in concentration. Maximum η % for ANC-1 is 95.5% at 200 mgL^{-1} and no change in η % was observed above this concentration and thus it is chosen as optimum concentration. At higher concentration value of η % is high and C_R is low, which is because more surface area covered by inhibitor molecules. The order of inhibition efficiency of ANCs is as follows: ANC-1 > ANC-2 > ANC-3.

Table 3.1.2

Corrosion parameters for the N80 steel in 15% HCl containing various concentrations of ANCs at 308 K obtained from weight loss measurements

| Inhibitor | Concentration (mgL^{-1}) | C_R (mmy^{-1}) | η (%) |
|-----------|-------------------------------------|-----------------------------|------------|
| 15% HCl | 0.0 | 22.44 | -- |
| ANC-1 | 50 | 18.15 | 19.1 |
| | 100 | 7.26 | 67.6 |
| | 150 | 3.30 | 85.2 |
| | 200 | 0.99 | 95.5 |
| ANC-2 | 50 | 19.73 | 12.0 |
| | 100 | 9.76 | 56.4 |
| | 150 | 5.47 | 75.5 |
| | 200 | 1.78 | 92.0 |
| ANC-3 | 50 | 20.46 | 8.8 |
| | 100 | 11.48 | 48.8 |
| | 150 | 7.39 | 67.0 |
| | 200 | 3.79 | 82.6 |

(ii) In order to find out the stability of protective film formed by the inhibitors, weight loss experiment was carried out in the temperature range of 308 to 338 K in absence and presence of optimum concentration (200 mg L^{-1}) of ANCs in 15% HCl. Figure 3.1.1 reveals that as the temperature increases corrosion rate (C_R) increases. This may occur

due to desorption of inhibitor molecules with an increase in temperature, which increases the contact of N80 steel with HCl.

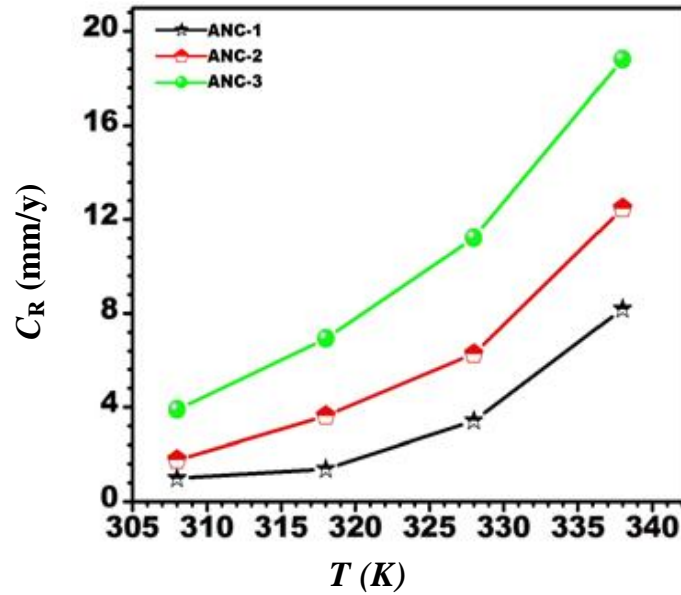


Figure 3.1.1: Variation of percentage inhibition efficiency of ANCs with temperature

3.1.2. Thermodynamic Parameters and Adsorption Considerations

The values of activation energy (E_a) can be calculated from the slopes of straight lines of $\log C_R$ versus $1/T$ plots. Figure 3.1.2 (a) shows the Arrhenius plots in the absence and presence of optimum concentration of ANCs at 308 K and it is found that almost all the regression coefficients (R^2) are close to 1, which means that the relationship between $\log C_R$ versus $1/T$ is linear. The values of E_a in the absence and presence of ANCs are tabulated in Table 3.1.3. The values of E_a in presence of ANCs are higher than in their absence, which provides an evidence for the strong adsorption of ANCs on the N80 steel surface [Negm *et al.* (2009); Solmaz *et al.* (2008)].

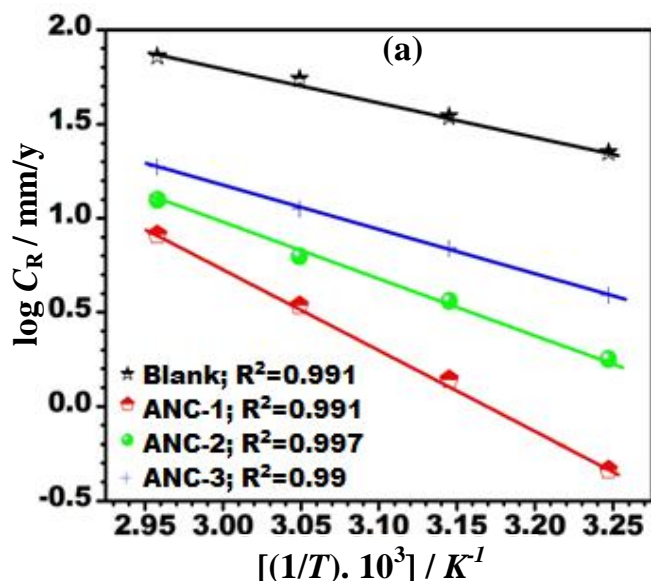


Figure 3.1.2 (a): Arrhenius plots of $\log C_R$ vs. $1000/T$ in absence and presence of ANCs

Table 3.1.3

Thermodynamic parameters for the adsorption of ANCs on N80 steel at optimum concentration in 15% HCl at 308 K

| Inhibitors | E_a (kJ mol ⁻¹) | K_{ads} ($\times 10^3 M^{-1}$) | $-\Delta G_{ads}^\circ$ (kJ mol ⁻¹) |
|------------|----------------------------------|---------------------------------------|--|
| Blank | 34.44 | – | – |
| ANC-1 | 82.33 | 3.25 | 31.00 |
| ANC-2 | 55.10 | 2.00 | 29.76 |
| ANC-3 | 44.96 | 1.48 | 28.98 |

The adsorption of ANCs can be confirmed by studying the adsorption isotherms. The adsorption isotherms give the basic information on the interaction of ANCs and N80 steel surface. By fitting the Langmuir adsorption isotherm, which is C/θ against C , straight lines were obtained and the values of R^2 are very much close to 1, which suggests that the adsorption of ANCs occurred by obeying Langmuir adsorption isotherm and are shown in Figure 3.1.2 (b). The values of equilibrium constant of adsorption (K_{ads}) and standard free energy of adsorption (ΔG_{ads}°) at 308 K are listed in Table 3.1.3. In general if the values of ΔG_{ads}° are less than -20 kJ mol^{-1} , the adsorption is considered as electrostatic

interactions between the charged molecules and the charged metal surface (physical adsorption). Those about -40 kJ mol^{-1} or higher involve charge sharing or a transfer from the inhibitor molecules to the metal surface to form a coordinate type of bond (chemical adsorption). The values of $\Delta G^{\circ}_{\text{ads}}$ in the present study indicate that the adsorptions of ANCs are both physisorption and chemisorption (mixed adsorption) [Hegazy *et al.* (2014)]. The values of K_{ads} can be calculated by using the intercepts of the straight lines and higher values of K_{ads} reveal stronger adsorption of ANCs over the N80 steel surface.

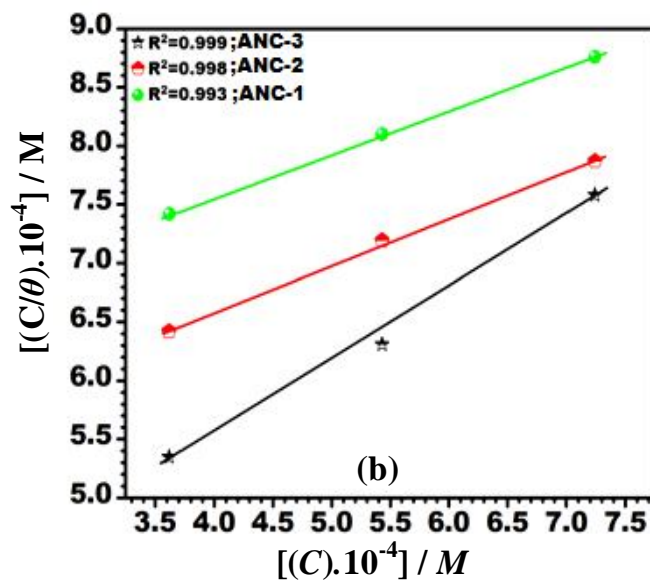


Figure 3.1.2 (b): Langmuir's isotherm plots for adsorption of ANCs on N80 steel surface

3.1.3. Electrochemical Impedance Spectroscopy

Electrochemical impedance spectroscopy is a rapid and convenient method to evaluate the inhibitive properties of the inhibitors [Hosseini *et al.* (2003)]. The Nyquist plots of N80 steel in absence and presence of optimum concentration (200 mgL^{-1}) of ANCs at 308 K are given in Figure 3.1.3 (a). Depressed semi-circles are observed indicating that the electrochemical reaction at solid/liquid interface has non-ideal capacitive behavior [Bentiss *et al.* (2004), Lebrini *et al.* (2006)]. Also, the presence of single time constant indicates that the corrosion process is mainly charge transfer

controlled [Anejjar *et al.* (2013)]. The shape of Nyquist plots in the absence and presence of ANCs are similar, which suggests that the corrosion mechanism remains unchanged [Anejjar *et al.* (2013)]. The only difference in the plots is that the diameters of the semicircle are larger in presence of ANCs than in their absence, which reveals that an enhancement occurs in the corrosion resistance of the N80 steel in presence of ANCs.

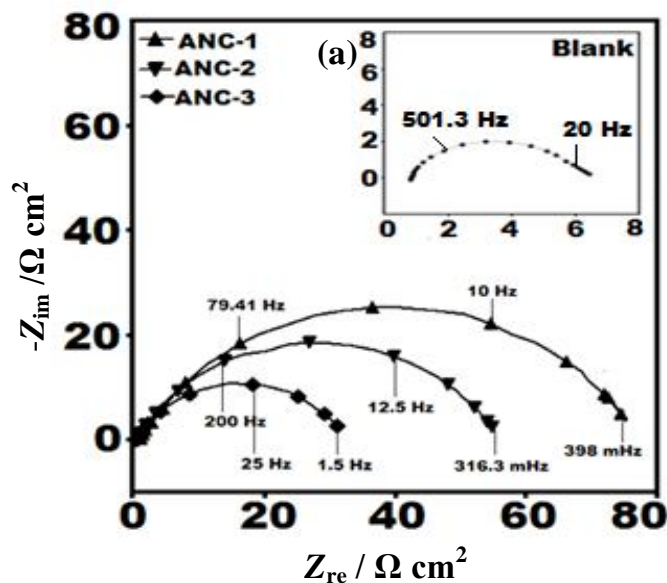


Figure 3.1.3 (a): Nyquist plots in absence and presence of optimum concentration of ANCs

Bode plots for N80 steel in absence and presence of ANCs are represented in Figure 3.1.3 (b). It is observed that in the presence of ANCs an increase in the low frequency impedance modulus occurs, which indicates the adsorptions of ANCs and increment in the corrosion resistance of N80 steel. The increase of phase angle in presence of ANCs indicates that there is only one time constant and is related to the electrical double layer formation at surface-solution interface [Motamedi *et al.* (2013)].

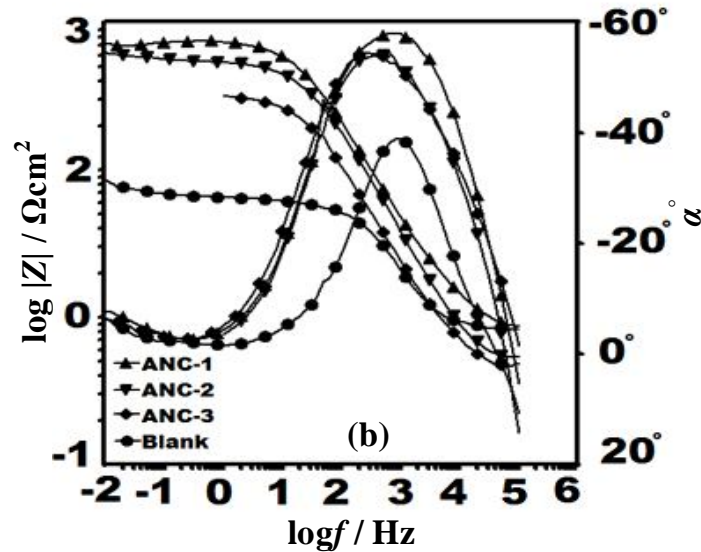


Figure 3.1.3 (b): Bode ($\log f$ vs. $\log |Z|$) and phase angle ($\log f$ vs. α°) plots in absence and presence of optimum concentration of ANCs

The impedance results were analyzed by using an equivalent circuit as shown in Figure 3.1.3 (c). This circuit contains R_s (solution resistance), R_{ct} (charge transfer resistance) and CPE (constant phase element) respectively.

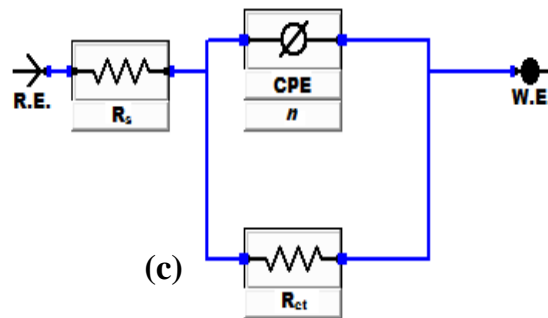


Figure 3.1.3 (c): Equivalent circuit used to fit the EIS data

Electrochemical impedance parameters are listed in Table 3.1.4, which reveals that the R_{ct} values in presence of ANCs are greater than in their absence. This increase in R_{ct} values is due to the surface area covered by the inhibitor molecules, which in turn increases the inhibition of N80 steel corrosion [John and Joseph (2012)]. However, a decrease in C_{dl} values occurs in presence of ANCs due to the adsorption of inhibitor

molecules over the N80 steel surface and which increases the thickness of the protective layer at the metal/solution interface [Li *et al.* (2012)].

Table 3.1.4

Electrochemical impedance parameters in absence and presence of optimum concentration (200 mg L⁻¹) of ANCs

| Inhibitors | R_{ct} ($\Omega \text{ cm}^2$) | n | Y_0 (μFcm^{-2}) | C_{dl} (μFcm^{-2}) | μ (%) |
|------------|---------------------------------------|-------|-----------------------------------|--------------------------------------|--------------|
| Blank | 4.58 | 0.755 | 603 | 134.2 | – |
| ANC-1 | 75.17 | 0.845 | 142 | 66.83 | 93.9 |
| ANC-2 | 53.75 | 0.823 | 194 | 79.26 | 91.4 |
| ANC-3 | 30.69 | 0.814 | 232 | 87.32 | 85.0 |

3.1.4. Potentiodynamic polarization

Figure 3.1.4, shows the polarization curves of N80 steel in the absence and presence of optimum concentration (200 mgL⁻¹) of ANCs at 308 K. In order to explain the kinetics of the corrosion, various electrochemical parameters, i.e., corrosion potential (E_{corr}), corrosion current density (I_{corr}), anodic Tafel slopes (β_a), cathodic Tafel slopes (β_c) and inhibition efficiency ($\eta\%$) values were calculated.

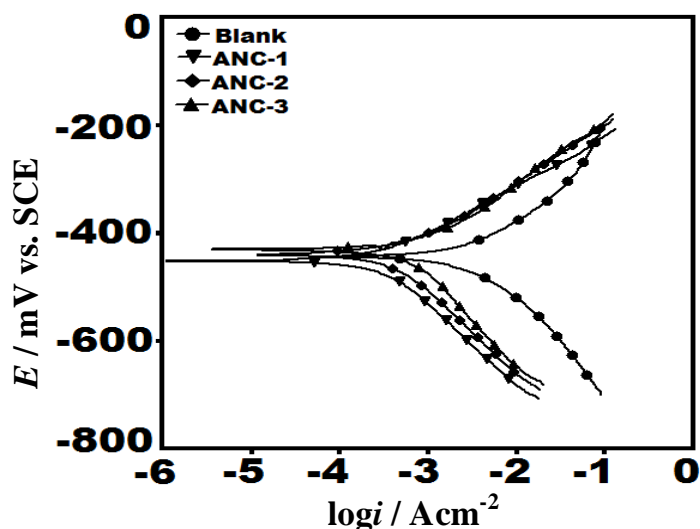


Figure 3.1.4: Potentiodynamic polarization curves in absence and presence of optimum concentration of ANCs

Figure 3.1.4 reveals that in presence of inhibitors both anodic and cathodic curves were shifted towards lower current density, which reveals that both anodic and cathodic corrosion reactions are retarded in presence of ANCs. Thus, ANCs are mixed type inhibitors. [Shen *et al.* (2006), Oguzie (2007)]. From Table 3.1.5, the values of β_a not changed very much with the addition of ANCs. However there is significant change in the values of β_c in presence of ANCs. The E_{corr} values were shifts towards more negative direction with respect to blank, which suggests the cathodic dominance of ANCs. So, it could be concluded that ANCs are mixed type inhibitors but predominantly cathodic [Xu *et al.* (2013), Tang *et al.* (2013)].

Table 3.1.5

Potentiodynamic polarization parameters in absence and presence of optimum concentration (200 mg L⁻¹) of ANCs

| Inhibitor | E_{corr} (mV/SCE) | I_{corr} ($\mu\text{A}/\text{cm}^2$) | β_a (mV/dec) | β_c (mV/dec) | η (%) |
|------------------|---|---|--|--|----------------------------------|
| Blank | -443 | 3201 | 85.7 | 100.8 | -- |
| ANC-1 | -450 | 313 | 91.9 | 151.7 | 90.2 |
| ANC-2 | -447 | 414 | 91.1 | 169.8 | 87.0 |
| ANC-3 | -446 | 617 | 93.0 | 191.9 | 80.7 |

3.1.5. Surface Analysis: SEM-EDX

SEM images of N80 steel in 15% HCl in absence and presence of optimum concentration (200 mgL⁻¹) of ANC-1 and ANC-2 after 6h immersion time at 308 K are shown in Figure 3.1.5 (a-c). Inspection of Figure 3.1.5 (a) reveals a very rough and highly corroded surface in absence of ANCs. However in presence of ANCs surface becomes smoother [Figure 3.1.5 (b, c)]; especially in the case of ANC-1 the surface is much smoother as compared to ANC-2.

The EDX images in absence and presence of ANC-1 and ANC-2 are given in Figure 3.1.5 (d-f). An observation of Figure 3.1.5 (d) shows the absence of oxygen (O) peak in absence of inhibitor, indicating the dissolution of oxide layer. But in presence of ANC-1 and ANC-2 an additional peak of nitrogen (N) is observed [Figure 3.1.5 (e, f)], which confirms the adsorption of ANCs.

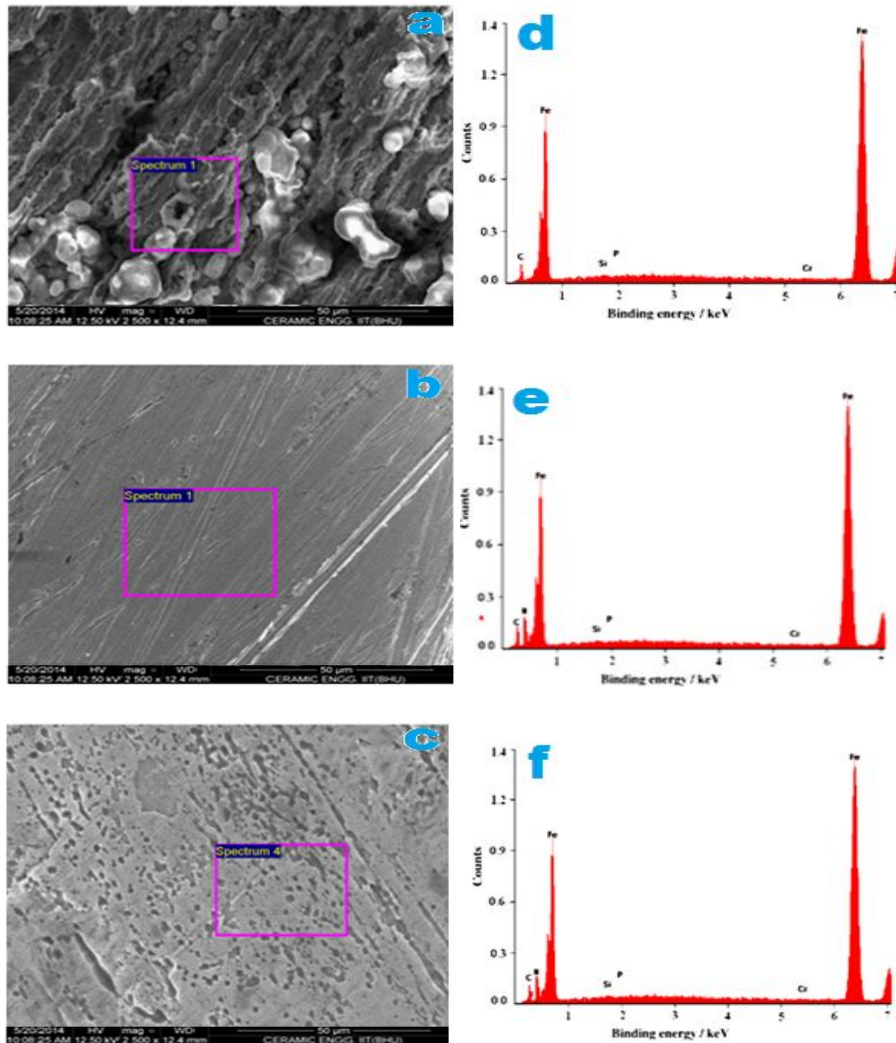


Figure 3.1.5: SEM micrographs of N80 steel (a) blank 15% HCl (b) ANC-1 (c) ANC-2 EDX spectra of N80 steel (d) blank 15% HCl (e) ANC-1 (f) ANC-2

3.1.6. Quantum chemical studies

(i) Neutral molecule

The inhibition property of an inhibitor depends upon its molecular arrangement in space and electronic structures [Talati and Gandhi, *et al.* (1983)]. The quantum chemical calculation gives an idea about the mechanism of inhibitor action and recently a large number of articles have been published focusing on the corrosion study by the use of quantum chemical calculations [Gece (2008)]. The optimized structures, HOMO and LUMO of neutral ANCs are shown in Figure 3.1.6 (a-c) and Figure 3.1.7 (a-c) respectively.

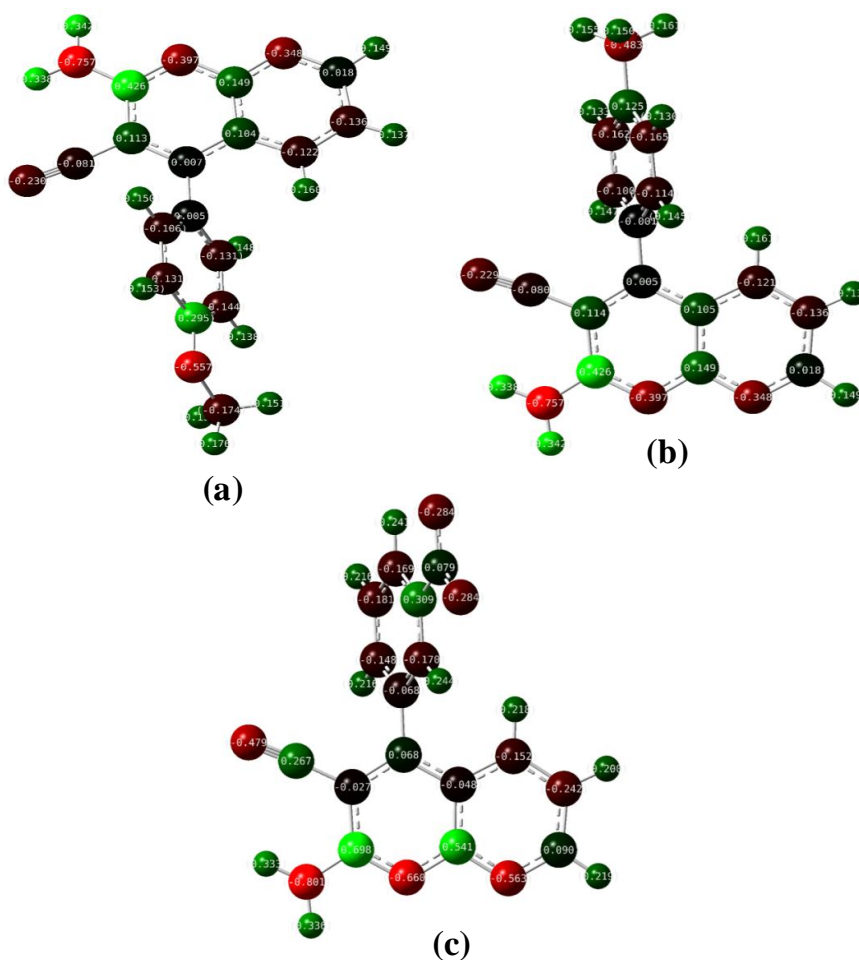


Figure 3.1.6: Optimized structures (a) ANC-1 (b) ANC-2 (c) ANC-3

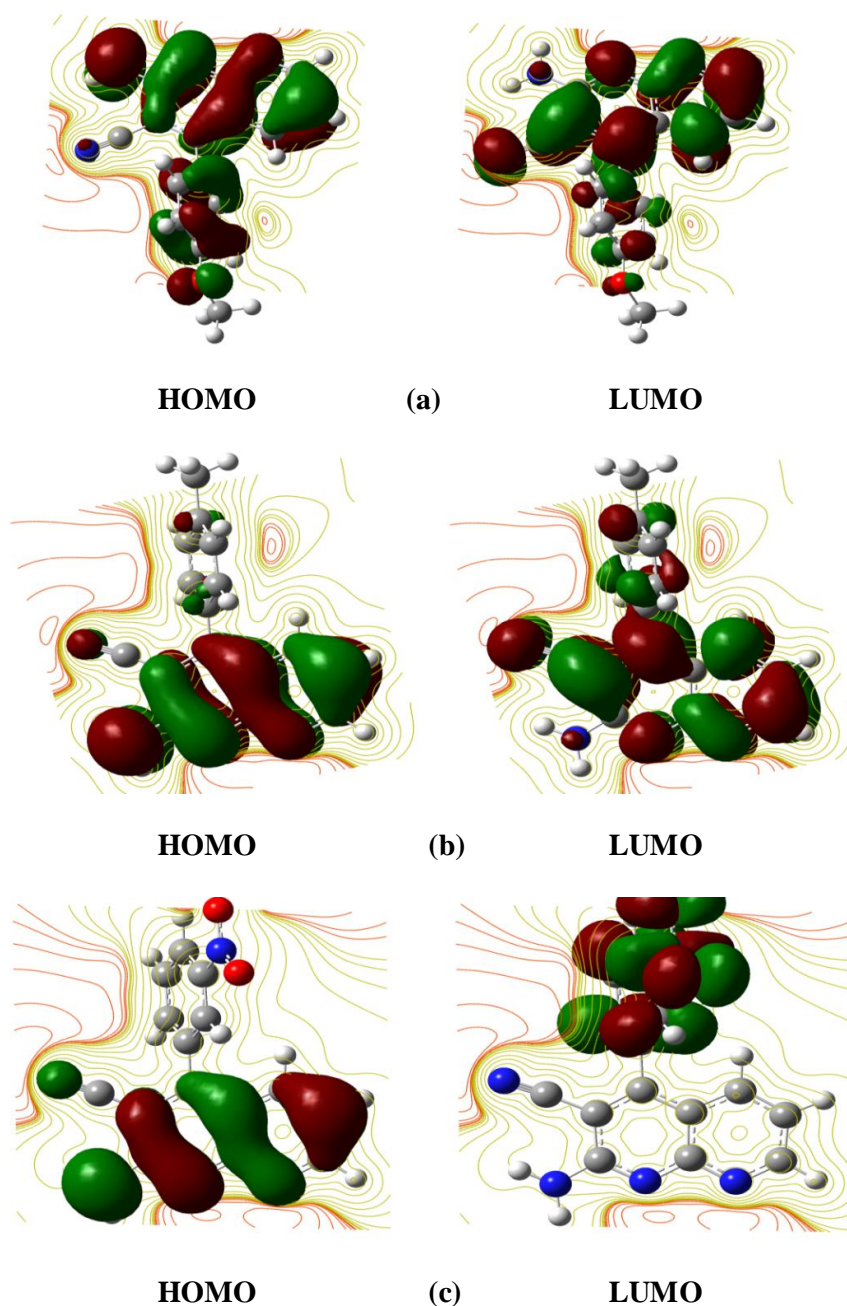


Figure 3.1.7: Frontier molecular orbital's of neutral (a) ANC-1 (b) ANC-2 (c) ANC-3

The ability of an inhibitor to donate its electrons to the metal surface is associated with the E_{HOMO} values, i.e. higher the E_{HOMO} values, easier will be the donation of electrons from the inhibitor to an empty metal d-orbitals. On the other hand, ability of inhibitor molecules to accept the electrons is associated with the E_{LUMO} values, i.e. lower

its value, easier will be the accommodation of additional negative charge by inhibitor molecules, which is given by filled metal d-orbitals. Also stability index of an inhibitor is related to the energy difference between E_{HOMO} and E_{LUMO} i.e. ΔE . Thus, lower the ΔE values, higher will be the stability of inhibitor and metal surface interaction. [Gao and Liang (2007)]. The quantum chemical parameters i.e. E_{HOMO} , E_{LUMO} , and ΔE are listed in Table 3.1.6.

Table 3.1.6

Calculated quantum chemical parameters of neutral and protonated ANC's

| Inhibitors | E_{HOMO} (eV) | E_{LUMO} (eV) | ΔE (eV) |
|------------|---------------------------|---------------------------|--------------------|
| ANC-1 | -4.218 | -2.117 | 2.101 |
| ANC-2 | -4.424 | -2.105 | 2.319 |
| ANC-3 | -5.295 | -2.084 | 3.211 |
| *ANC-1 | -10.198 | -8.779 | 1.419 |
| *ANC-2 | -10.347 | -8.314 | 2.033 |
| *ANC-3 | -10.597 | -8.101 | 2.496 |

*ANC-1,*ANC-2 and ANC-* are protonated inhibitors

It is evident that the E_{HOMO} values are as follows: ANC-1> ANC-2> ANC-3, which suggests that the electron donation ability of ANC-1 is highest and it will adsorb with a greater extent over N80 steel surface, thus providing the highest inhibition efficiency. In the same way E_{LUMO} values are in the order: ANC-3> ANC-2> ANC-1. A lower value of ANC-1 indicates its ability to accept electrons thereby reducing the corrosion of N80 steel to a greater extent [Ghailane *et al.* (2013)]. Also the ΔE value of ANC-1 is lowest, which suggests its higher adsorptive ability than ANC-2 and ANC-3. Thus, the order of protection of N80 steel in 15% HCl is as follows: ANC-1> ANC-2 >ANC-3.

(ii) Protonated molecule

In aqueous acidic media, there is the possibility of the inhibitor to undergo protonation. These protonated ANC's get adsorbed over the N80 steel surface. Thus, the most electronegative site has been protonated and their molecular properties are reported in Table 3.1.6. The HOMO and LUMO images of preferred protonated sites are shown in Figure 3.1.8 (a-c). The ΔE values in protonated ANC's are less in comparison to neutral one (Table 3.1.6), suggesting that protonated ANC's have more adsorption ability with N80 steel than neutral one.

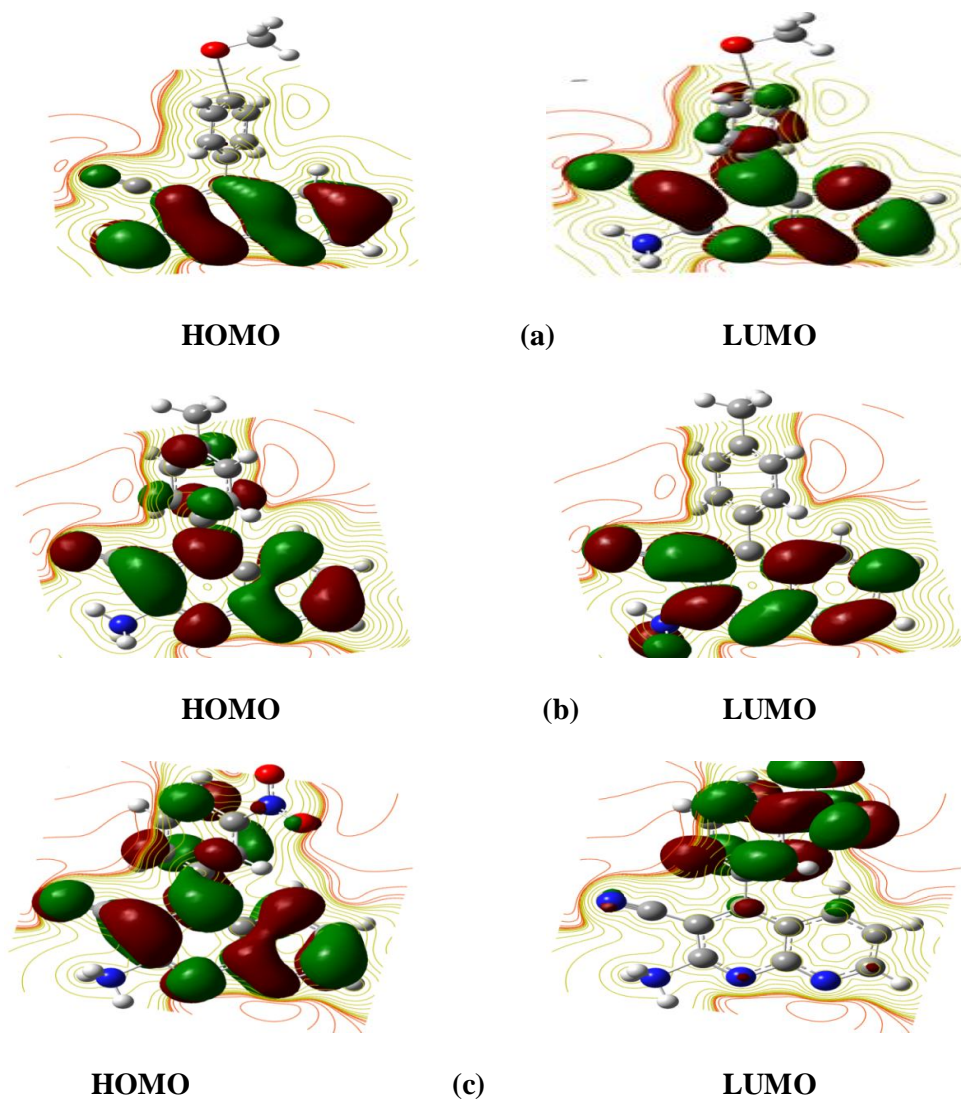


Figure 3.1.8: Frontier molecular orbitals of protonated (a) ANC-1 (b) ANC-2 (c) ANC-3

3.1.7. Explanation of inhibition mechanism

Organic molecules are adsorbed on the metal either physically or chemically or in a combination of both. In the case of physical adsorption, electrostatic interaction occurs between charged metal surface and charged inhibitor molecules. In chemical adsorption, inhibition occurs by donor-acceptor interactions between lone pair electrons on the heteroatoms (N and O), π -electrons of multiple bonds as well as phenyl group with vacant d-orbitals of Fe [Behpour *et al.* (2008)]. In the present case, the values of adsorption free energy range between -20 and -40 kJ mol⁻¹, which indicates that the ANCs molecules adsorb in a combination of both physical and chemical adsorption. It is experimentally proved that in acidic solution steel surface is positively charged (Figure 3.1.9). So, initially Cl⁻ ions may get adsorbed on positively charged N80 steel surface, and then the adsorption of protonated ANCs molecules occurs via electrostatic interactions (physical adsorption), which leads to the formation of protective (FeCl⁺ANCs⁺)_{ads} layer. But at the same time, lone pair of electrons on heteroatoms, π -electrons in naphthyridine and benzene ring are donated to vacant 3d-orbitals of iron atoms (chemical adsorption). Also the filled orbitals of N80 steel can give their electrons to vacant orbitals of ANCs molecules through retrodonation.

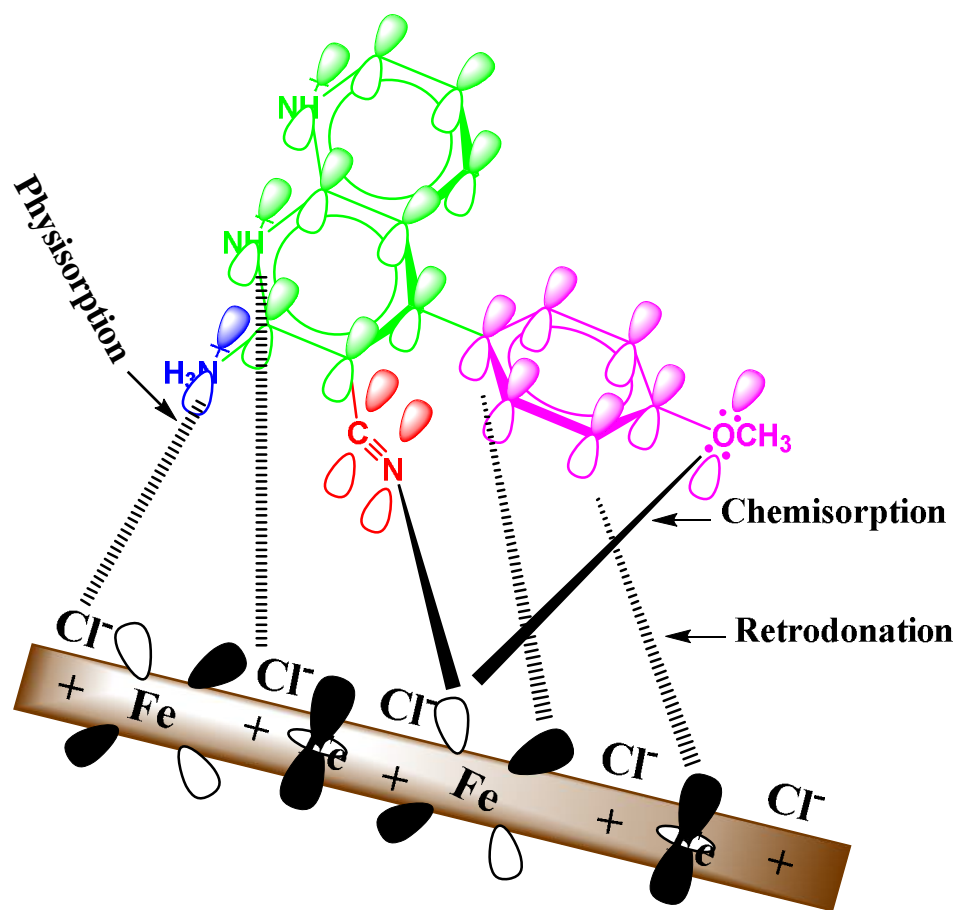


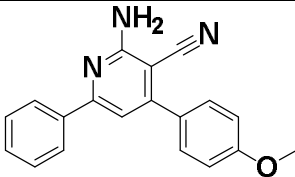
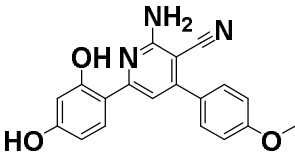
Figure 3.1.9: Plausible adsorption model of ANC-1 on to N80 steel surface in HCl

3.2. Pyridine derivatives as Corrosion Inhibitors

Pyridine derivatives are one of the important classes of compounds having various pharmacological properties such as antioxidant, anti-atherosclerosis, anti-tumor, anti-mutagenic, anti-diabetic, neuromodulator, anti-vasodilator, hepatoprotector, neuroprotector and memory enhancer [Lembège *et al.* (1996)]. The literature survey reveals that several pyridine derivatives were used as corrosion inhibitors, but they were effective at higher inhibitor and lower acid concentrations respectively [Ghazoui *et al.* (2012), Mert *et al.* (2014), Doddahosuru *et al.* (2014), Krim *et al.* (2009), Yıldız *et al.* (2014), Abd El-Maksoud and Fouada (2005), Li *et al.* (2014)].

The present study deals with the study of inhibition effect of two pyridine derivatives namely 2-amino-6-(2,4-dihydroxyphenyl)-4-(4-methoxyphenyl) nicotinonitrile (ADP) and 2-amino-4-(4-methoxyphenyl)-6-phenylnicotinonitrile (AMP) on N80 steel in 15% HCl using weight loss measurements, potentiodynamic polarization measurements, electrochemical impedance spectroscopy, quantum chemical calculations, Scanning electron microscopy (SEM) and Scanning electrochemical microscopy (SECM). The molecular structure, abbreviations and IUPAC name of the synthesized pyridine derivatives are given in Table 3.2.1.

Table 3.2.1 The IUPAC Name, molecular structure and abbreviation of pyridine derivatives used

| S.No. | IUPAC Name | Molecular Structure | Abbreviation |
|-------|---|--|--------------|
| 1 | 2-amino-4-(4-methoxy phenyl)-6-phenyl nicotinonitrile |  | AMP |
| 2 | 2-amino-6-(2,4-dihydroxyphenyl)-4-(4-methoxy phenyl)nicotinonitrile |  | ADP |

3.2.1. Weight loss measurements

(i) The corrosion rate (C_R) of N80 steel as a function of inhibitors (ADP and AMP) concentration in 15% HCl was determined at 308 K and summarized in Table 3.2.2. It is clear from table that with increase in inhibitor concentration, inhibition efficiency (η %) increases and corrosion rate decreases. The lowest C_R (2.11 $\text{mm}y^{-1}$) and highest η % (90.5%) were obtained for ADP at 200 mgL^{-1} , and this concentration was found to be optimum because above this concentration no significant change was observed in efficiency. From the Table 3.2.2, it is clear that the order of inhibition efficiency is as follows: ADP > AMP

Table 3.2.2

Corrosion parameters for the N80 steel in 15% HCl containing various concentrations of inhibitors at 308 K obtained from weight loss measurements

| Inhibitor | Concentration (mgL^{-1}) | C_R ($\text{mm}y^{-1}$) | η (%) |
|-----------|-------------------------------------|-----------------------------|------------|
| 15% HCl | 0.0 | 22.44 | |
| ADP | 50 | 14.71 | 34.4 |
| | 100 | 8.84 | 58.9 |
| | 150 | 4.48 | 77.1 |
| | 200 | 2.11 | 90.5 |
| AMP | 50 | 16.76 | 25.2 |
| | 100 | 10.16 | 54.7 |
| | 150 | 5.61 | 73.0 |
| | 200 | 2.97 | 86.7 |

(ii) The corrosion rate (C_R) was studied in the temperature range of 308 to 338 K in 15% HCl following an immersion period of 6h, at optimum concentration (200 mgL^{-1}) of inhibitors and the results obtained are shown in Figure 3.2.1. The C_R increases as the temperature increases. This increase in C_R is attributed to desorption of the inhibitor molecules from the N80 steel surface.

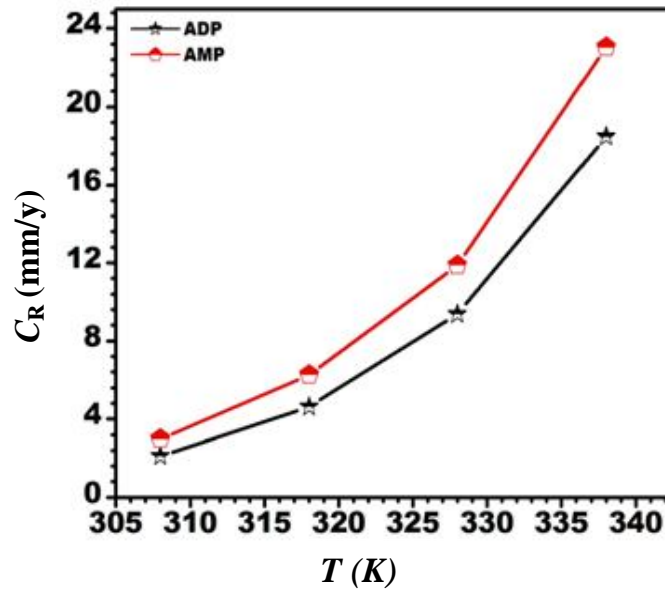


Figure 3.2.1: Variation of percentage inhibition efficiency of inhibitor with temperature

3.2.2. Thermodynamic Parameters and Adsorption Considerations

Figure 3.2.2 (a) represents the Arrhenius plots between $\log(C_R)$ and $1/T$. From the slope of the straight line, [Figure 3.2.2(a)] activation energy (E_a) was calculated. In presence of inhibitors, E_a values (Table 3.2.3) increases, indicating that the adsorption is physical [Anejjar *et al.* (2013), Xu *et al.* (2013)]. Solely E_a cannot make the interpretation of adsorption type because there is a competition occurring between inhibitor and water molecules for adsorption on the surface of metal, and removal of water molecules from the surface requires some activation energy [Vracar and Drazic (2002)]. Therefore, the adsorption of ADP and AMP molecules on the N80 steel surface in 15% HCl takes place through both physical and chemical processes simultaneously [Tang *et al.* (2013)].

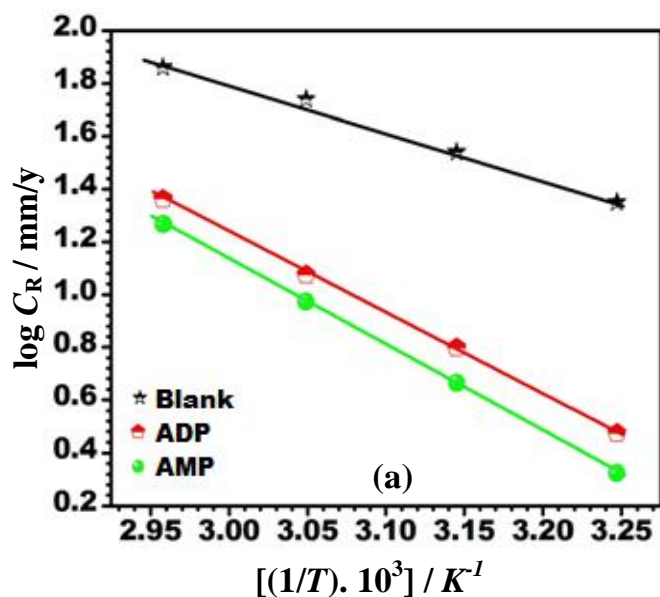


Figure 3.2.2 (a): Arrhenius plots of $\log C_R$ vs. $1000/T$ in absence and presence of inhibitor

To obtain the adsorption isotherm, fractional surface covered values (θ) by the inhibitor molecules as a function of their concentration are determined. The Langmuir adsorption isotherm (C/θ versus C) provides the best fit [Figure 3.2.2 (b)]. The values of regression coefficients (R^2) of ADP and AMP are nearly approaching towards 1, thereby confirming that their adsorption follows the Langmuir's isotherm. K_{ads} values can be calculated from the intercepts of the straight lines and the obtained data are given in Table 3.2.3. The values of K_{ads} are large, which confirmed the strong adsorption of ADP and AMP on the N80 steel surface. The large negative value of ΔG_{ads}° (Table 3.2.2) suggests strong interactions between the inhibitor molecules and the metal surface [Bayol *et al.* (2008), Bahrami *et al.* (2010)]. Generally, if the value of ΔG_{ads}° is -40 kJ mol^{-1} or more negative, the process could be understood as chemical adsorption, which is sharing of charge in between inhibitor molecules and metals in order to form a co-ordinate covalent bond. However, the adsorption is physical if the value of ΔG_{ads}° is equal to or lower than -20 kJ mol^{-1} , which is an electrostatic interaction between the inhibitor molecules and

metal surface [Golestani *et al.* (2014), Abiola and Oforka (2004)]. The obtained values of $\Delta G^{\circ}_{\text{ads}}$ for ADP and AMP in the present study are more than -20 kJ mol^{-1} and less than -40 kJ mol^{-1} (Table 3.2.3), therefore, their adsorption could be considered as a mixture of both physical and chemical [Li *et al.* (2011)].

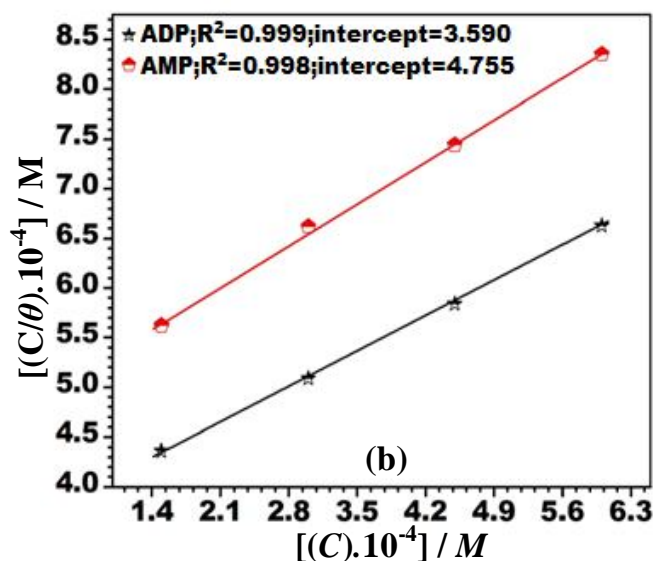


Figure 3.2.2 (b): Langmuir's isotherm plots for adsorption of inhibitors

Table 3.2.3

Thermodynamic parameters for the adsorption of inhibitors on N80 steel at different concentrations in 15% HCl at 308 K

| Inhibitors | E_a (kJ mol^{-1}) | K_{ads} ($\times 10^3 \text{ M}^{-1}$) | $-\Delta G^{\circ}_{\text{ads}}$ (kJ mol^{-1}) |
|------------|-----------------------------------|--|--|
| Blank | 34.44 | — | — |
| ADP | 62.30 | 2.78 | 30.60 |
| AMP | 58.57 | 2.10 | 29.88 |

3.2.3. Electrochemical Impedance Spectroscopy

Nyquist plots in absence and presence of optimum concentration (200 mgL^{-1}) of inhibitors (ADP and AMP) at 308 K are shown in Figure 3.2.3 (a) and their corresponding calculated parameters are given in Table 3.2.4.

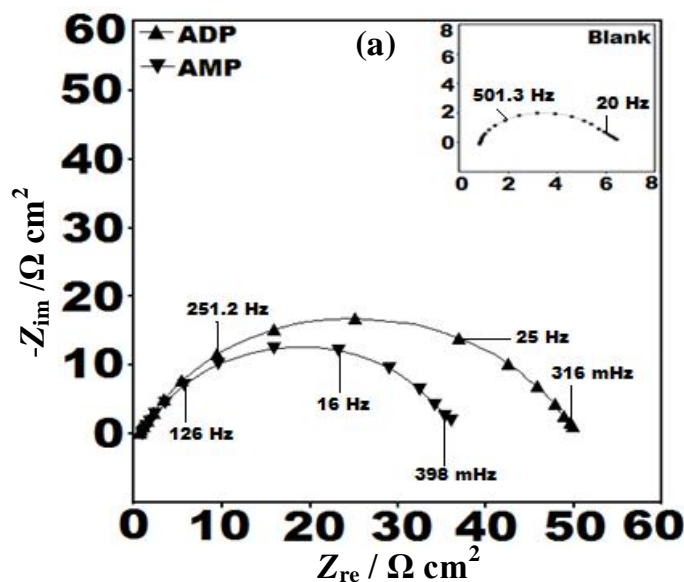


Figure 3.2.3 (a): Nyquist plots in absence and presence of optimum concentration of inhibitors

Table 3.2.4

Electrochemical impedance parameters in absence and presence of optimum concentration (200 mg L^{-1}) of inhibitors

| Inhibitors | R_{ct} ($\Omega \text{ cm}^2$) | n | Y_0 (μFcm^{-2}) | C_{dl} ($\mu\text{F cm}^{-2}$) | η (%) |
|------------|---------------------------------------|-------|-----------------------------------|---------------------------------------|---------------|
| Blank | 4.58 | 0.755 | 603 | 134.2 | – |
| ADP | 48.88 | 0.885 | 89 | 48.1 | 90.63 |
| AMP | 35.09 | 0.822 | 173 | 73.0 | 86.94 |

From Figure 3.2.3 (a), it is obvious that the obtained plots are depressed semi-circles having their center located under the real axis, and their diameters are increased in the presence of the optimum concentration of inhibitors. Thus, it could be said that the corrosion is being controlled by charge transfer process [Lebrini *et al.* (2006), Bentiss *et al.* (2004)]. A higher charge transfer value in the presence of inhibitors in comparison to blank is associated with decrease in the corrosion process. The equivalent circuit used to fit the impedance data is given in Figure 3.2.3 (b). This circuit consists of electrolyte resistance (R_s), charge transfer resistance (R_{ct}) and constant phase element (CPE).

Simulated plots of Nyquist and Bode of ADP were constructed to check fitness accuracy of the used circuit and are shown in Figure 3.2.3 (c-d).

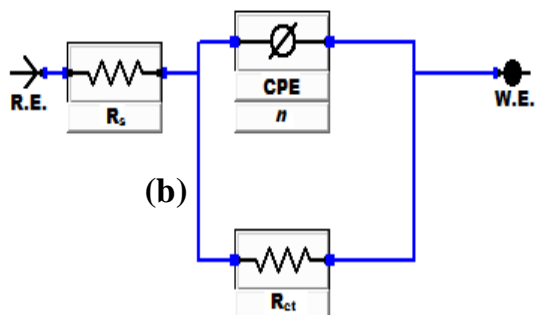


Figure 3.2.3 (b): Equivalent circuit used to fit the EIS data

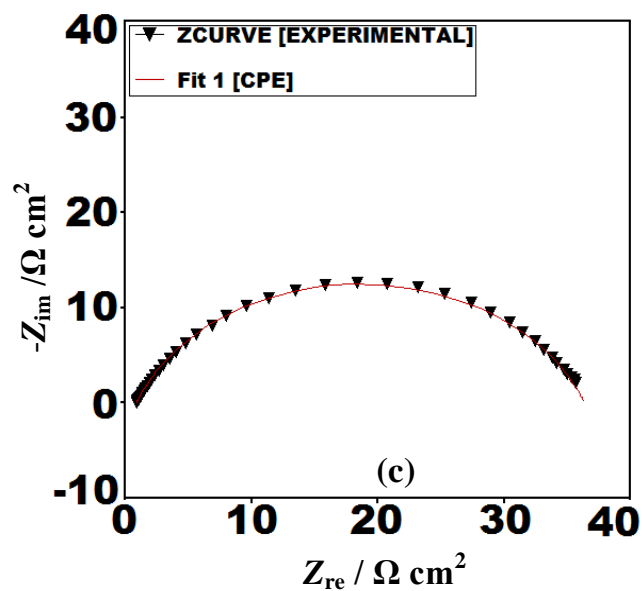


Figure 3.2.3 (c): Simulated Nyquist plot

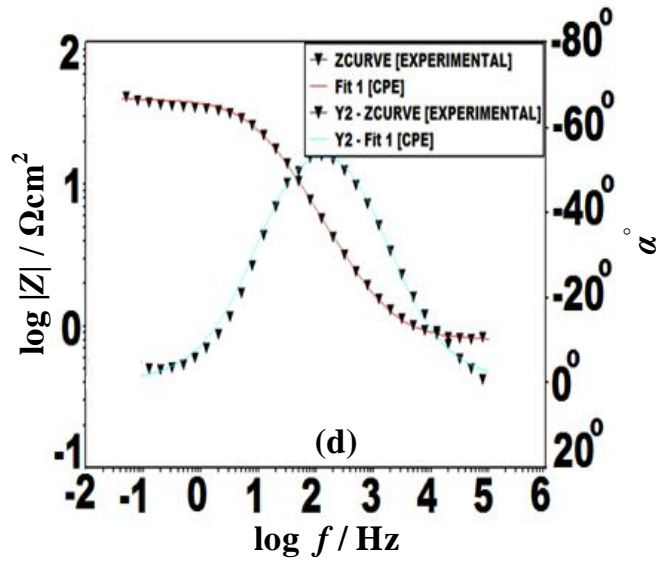


Figure 3.2.3 (d): Simulated Bode plot

The combined Bode and phase angle plots in absence and presence of the optimum concentration of inhibitors are shown in Figure 3.2.3 (e).

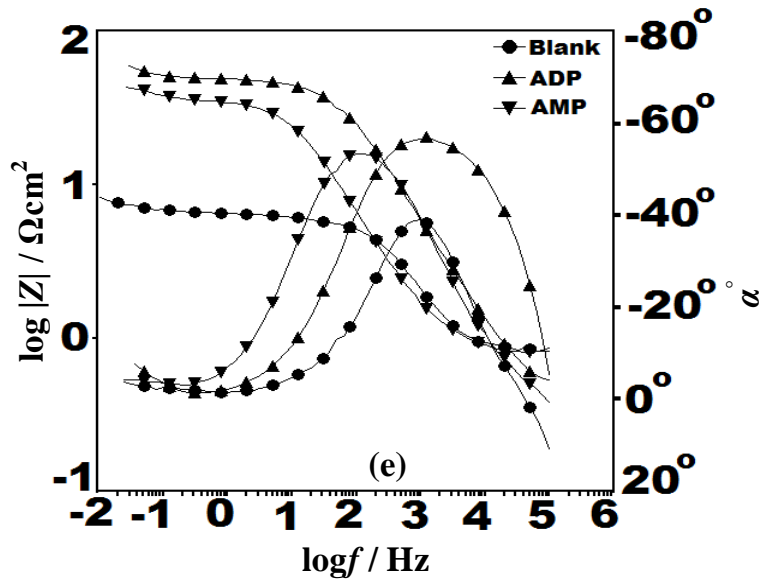


Figure 3.2.3 (e): Bode ($\log f$ vs. $\log |Z|$) and phase angle ($\log f$ vs. α) plots in absence and presence of optimum concentration of inhibitors

At the lower frequency the impedance values increased in presence of inhibitors, which confirms their adsorption and protection of N80 steel from corrosion [Mahdavian and Ashhari (2010)]. In the phase angle plots at intermediate frequency the values of phase angle increased in presence of inhibitors, which is related to the double layer

formation at electrode-solution interface [Motamedi *et al.* (2013)]. In presence of inhibitors C_{dl} value tends to decrease because of decrease in local dielectric constant and/or an increase in the thickness of the electrical double layer.

3.2.4. Potentiodynamic polarization

Potentiodynamic polarization curves in absence and presence of optimum concentration of ADP and AMP at 308 K are shown in Figure. 3.2.4.

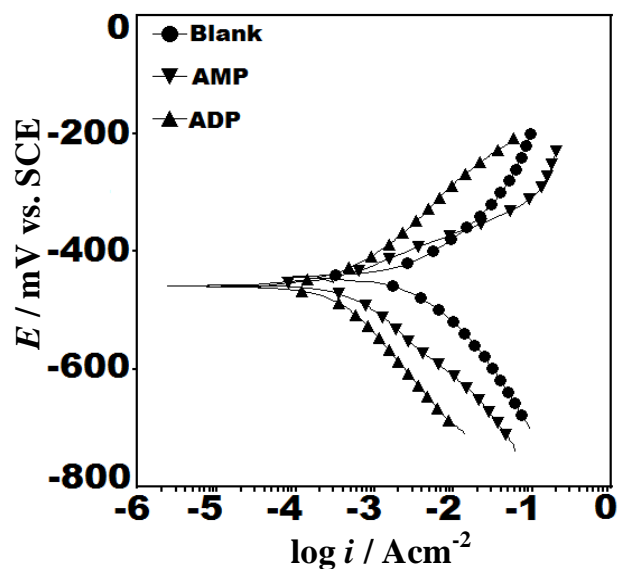


Figure 3.2.4: Potentiodynamic polarization curves in absence and presence of optimum concentration of inhibitors

The related parameters such as corrosion potential (E_{corr}), corrosion current density (I_{corr}), anodic and cathodic Tafel constant (β_a and β_c) were calculated and listed in Table 3.2.5. In presence of ADP and AMP corrosion current density is decreased, which confirms the inhibiting action of the used inhibitors [Obot *et al.* (2010)]. The values of β_a are almost constant in absence and presence of inhibitor but β_c values were significantly changed [Ansari *et al.* (2014), Negm *et al.* (2011)]. It is reported that if the displacement in E_{corr} (inhibited) is more than 85 mV from E_{corr} (blank), the inhibitor is called as cathodic or anodic type and if this displacement is less than 85 mV, the inhibitor is called as mixed type [Ferreira *et al.* (2004), Sorkhabi *et al.* (2004)]. In the present study, the

maximum displacement in E_{corr} value was 15 mV towards cathodic side, which indicates that ADP and AMP are mixed type inhibitors favoring the cathodic side.

Table 3.2.5

Potentiodynamic polarization parameters in absence and presence of optimum concentration (200 mg L^{-1}) of inhibitors

| Inhibitor | E_{corr} (mV/SCE) | I_{corr} ($\mu\text{A}/\text{cm}^2$) | β_a (mV/dec) | β_c (mV/dec) | η (%) |
|------------------|-------------------------------|--|-----------------------|-----------------------|---------------|
| Blank | -443 | 3201 | 85.7 | 100.8 | -- |
| ADP | -456 | 246 | 110 | 191 | 92.3 |
| AMP | -458 | 414 | 114 | 198 | 87.0 |

3.2.5. Surface Analysis: SEM and SECM

Figure 3.2.5 (a-c) represents the SEM images in the absence and presence of inhibitors at 308 K. In the absence of inhibitors, N80 steel surface was severely damaged (Figure 3.2.5 a), whereas, in the presence of ADP and AMP (Figure 3.2.5 b, c), the corrosion was tangibly suppressed. This nearly smooth morphology of N80 steel surface shows that the inhibitors protect the N80 steel effectively.

SECM images of N80 steel surface specimens in absence and presence of inhibitors (ADP and AMP) is shown in Figure 3.2.5 (d-f).

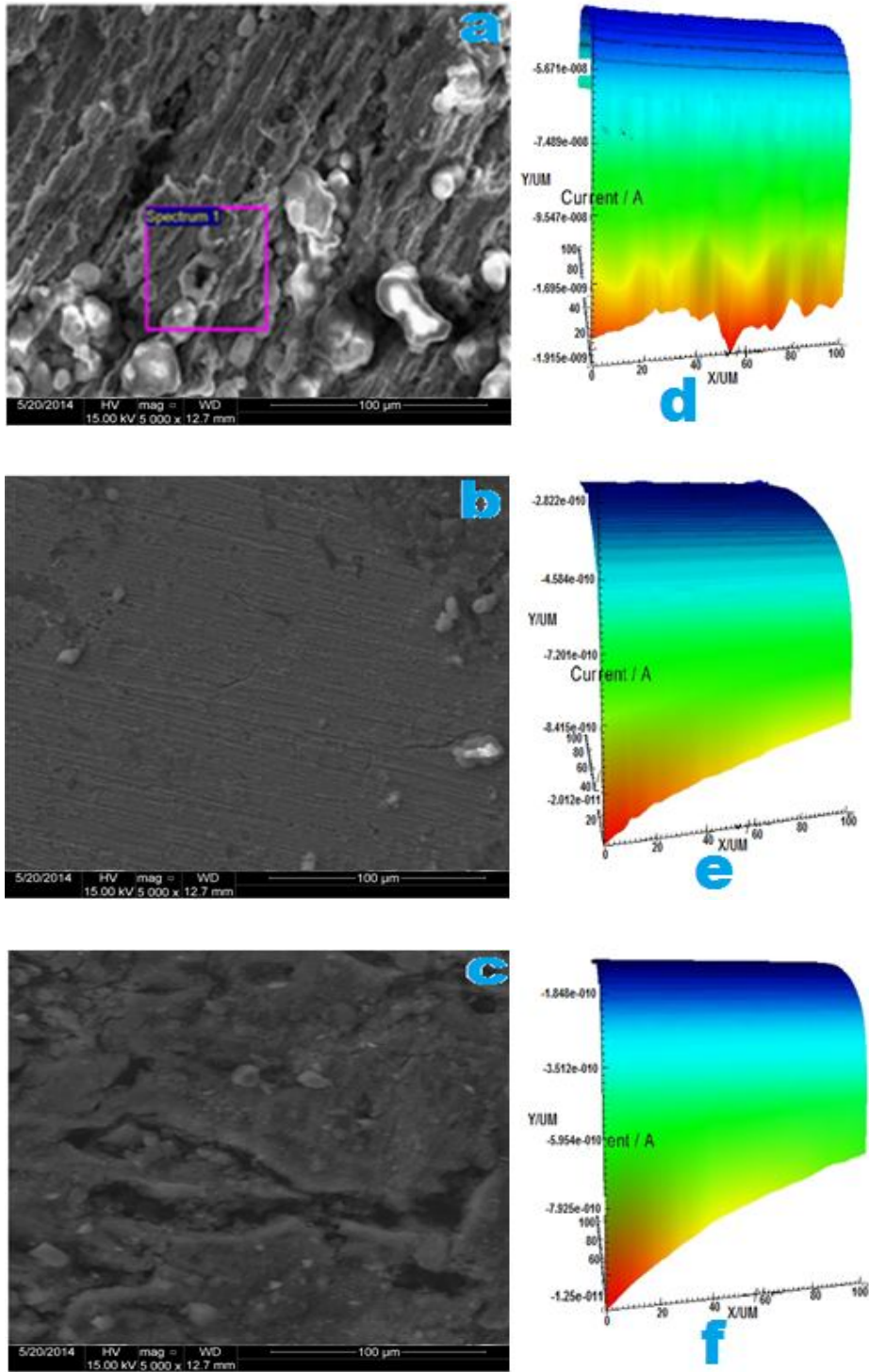


Figure 3.2.5: SEM micrographs of N80 steel (a) blank 15% HCl (b) ADP (c) AMP
 SECM micrographs of N80 steel (d) blank 15% HCl (e) ADP (f) AMP

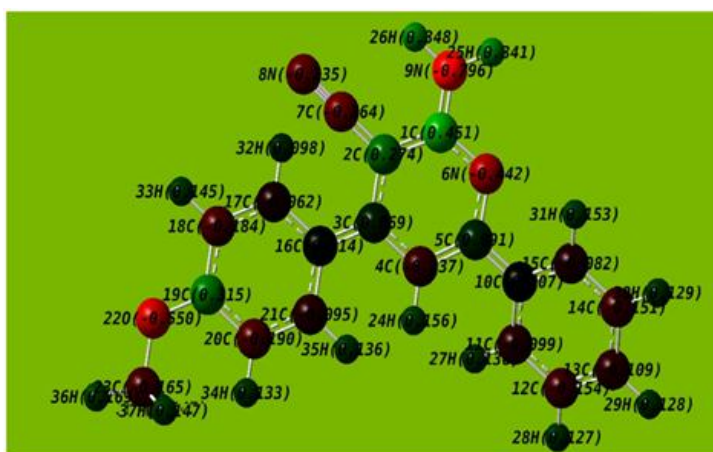
A negative feedback effect was observed when the probe tip was passed towards the metal surface on which a film of inhibitor was formed. This is due to the hindrance in the diffusion field surrounding the tip and thus the tip current decreases (Figure 3.2.5 e, f). But in the absence of inhibitor as the tip approaches towards the metal surface a positive feedback effect was observed in which the current was increased (Figure. 3.2.5 d), due to the conducting nature of the metal surface.

3.2.6. Quantum chemical study

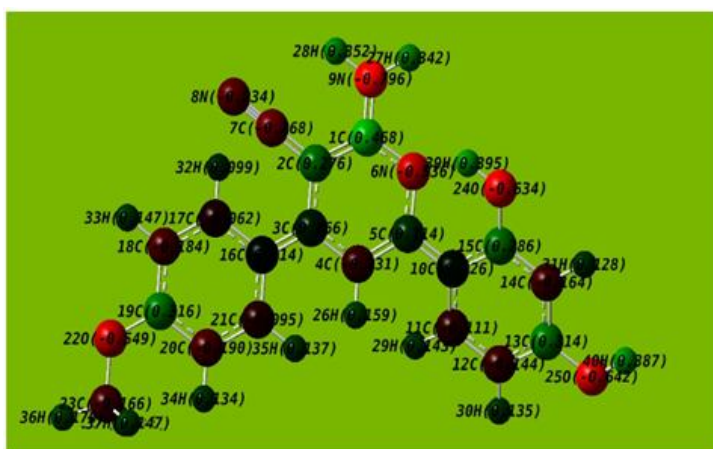
(i) Neutral molecule

The optimized geometry, HOMO and LUMO structures of studied inhibitors (ADP and AMP) are given in Figure 3.2.6 (a-b) and Figure 3.2.7 (a-d) respectively. As per the frontier molecular orbital theory, HOMO energy is connected with the ability to donate the electron to the empty d-orbital of metal surface i.e. higher its value greater would be its donation ability. However, LUMO energy is connected to the ability for electron acceptance i.e. lower its value higher would be its electron accepting tendency from the filled metal orbitals [Zor *et al.* (2011)]. The difference between E_{HOMO} and E_{LUMO} , referred as the energy gap (ΔE), which is also an important parameter to determine the inhibition efficiency of the inhibitors, i.e. lower the ΔE values of the inhibitor, higher would be its inhibition efficiency. As from the Table 3.2.6, the values of E_{HOMO} are in the order: ADP > AMP. A higher value in case of ADP is due to the presence of electron donor -OH groups on the phenyl ring. Thus, ADP acts as a better inhibitor as compared to AMP. The E_{LUMO} values are in the order of AMP > ADP. Thus, a lower value in case of ADP further emphasizes its better inhibition efficiency. In addition, ADP has lower ΔE values, which indicate its higher reactivity and more inclination to adsorb on the metal surface. Therefore, the inhibition capacity of the studied inhibitors are ADP > AMP, which is in agreement with the experimentally obtained data. The

negative Mulliken charges (Table 3.2.7) on heteroatoms show their greater electron donation capacity [Xia *et al.* (2008)].



(a)



(b)

Figure 3.2.6: Optimized structures (a) AMP (b) ADP

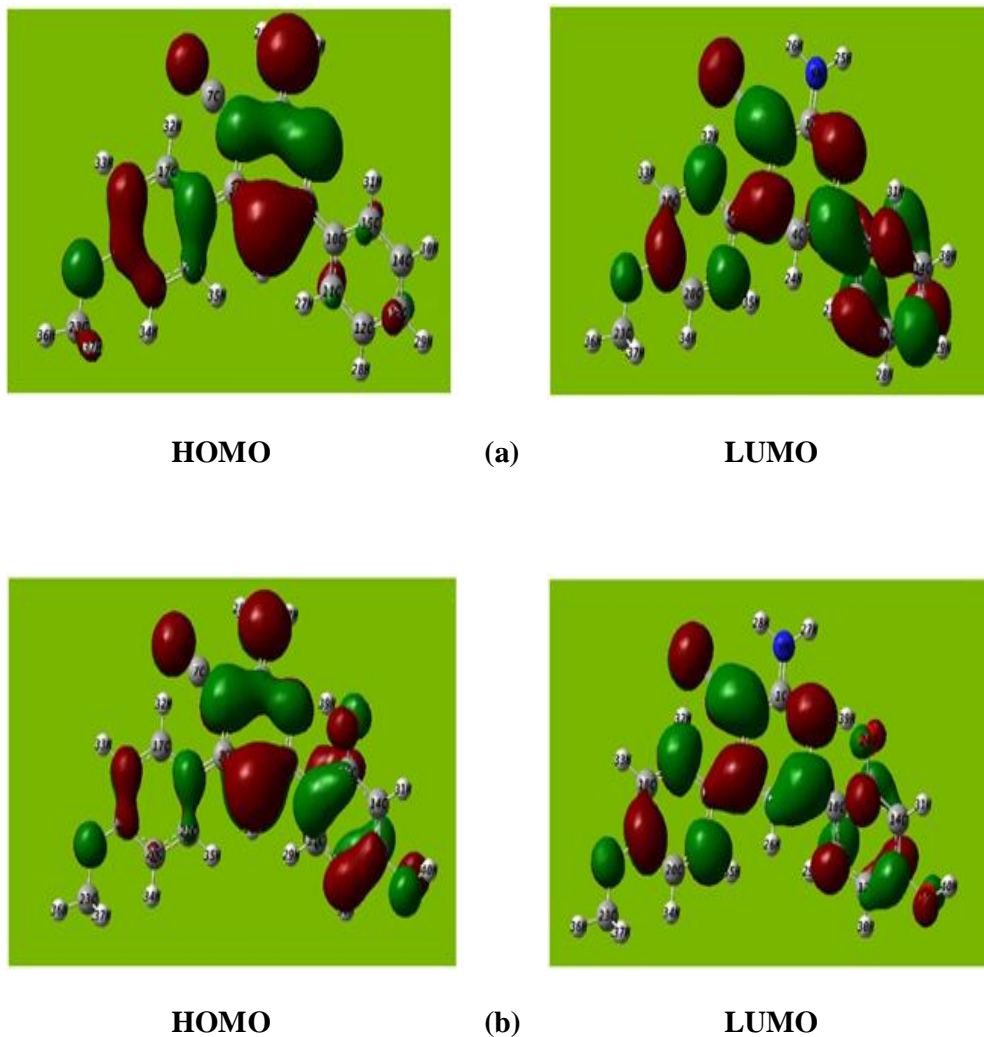


Figure 3.2.7: Frontier molecular orbitals (a) AMP (b) ADP

Table 3.2.6

Calculated quantum chemical parameters of neutral and protonated inhibitors

| Inhibitors | E_{HOMO} (eV) | E_{LUMO} (eV) | ΔE (eV) |
|------------------|---------------------------|---------------------------|--------------------|
| ADP | -5.523 | -1.850 | 3.673 |
| AMP | -5.659 | -1.798 | 3.836 |
| ADP ⁺ | -2.867 | -0.882 | 1.985 |
| AMP ⁺ | -3.254 | -0.236 | 3.018 |

ADP⁺ and AMP⁺ are protonated inhibitors

Table 3.2.7

Mulliken charges on hetroatoms and proton affinity values

| Inhibitors | Mulliken charges on heteroatoms | | | | | | PA (kcal/mol) | | |
|------------|---------------------------------|----------------|----------------|-----------------|-----------------|-----------------|------------------|-----------------|-----------------|
| | N ₆ | N ₈ | N ₉ | O ₂₂ | O ₂₄ | O ₂₅ | N ₉ | O ₂₂ | O ₂₅ |
| ADP | -0.535 | -0.234 | -0.796 | -0.548 | -0.634 | -0.642 | -357.13 | -- | -330.68 |
| AMP | -0.414 | -0.235 | -0.796 | -0.549 | -- | -- | -359.77 | -329.36 | -- |

(ii) Protonated inhibitors

In aqueous medium, the inhibitor molecules undergo protonation and these protonated species also get adsorbed on the N80 steel surface. Therefore, it is important to compare the electronic properties of the protonated species with that of the neutral one, to check which one would get adsorbed on the metal surface dominantly. In the studied inhibitors, there are many hetero-atoms, so the most favorable site will be the one which has the larger negative value i.e. N₉ and O₂₅ (in ADP) and N₉ and O₂₂ (in AMP). The preferential centre, which undergoes protonation, could be determined by comparing the proton affinity (*PA*) at N₉, O₂₂ and O₂₅. The proton affinity (*PA*) energy is estimated using following equation:

$$PA = E_{prot} + E_{H_2O} - E_{non-prot} + E_{H_3O^+}$$

where, E_{prot} and $E_{non-prot}$ are the total energies of the protonated and non-protonated inhibitors respectively, E_{H_2O} is the total energy of a water molecule and $E_{H_3O^+}$ is the total energy of hydronium ion. The preferential site for protonation to occur in both the inhibitors (ADP and AMP) is the N₉ atom (Table 3.2.7).

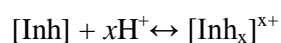
A comparison of the quantum chemical parameter of neutral and protonated inhibitors (Table 3.2.6) reveals that the E_{HOMO} values in both the inhibitors are higher in protonated form as compared to the neutral form. This indicates that the protonated

species have a greater tendency to donate the electrons and therefore to bind strongly on the N80 steel surface. In addition, the value of ΔE in protonated species is lower than the neutral one, which suggests that the protonated species is more reactive than the neutral species. Therefore, the protonated species are more likely to adsorb over the N80 steel surface than neutral species. The above discussion also supports the experimentally observed adsorption i.e. both physical and chemical.

3.2.7. Mechanism of inhibition

In the studied inhibitors based on their chemical structures, they have various active sites for adsorption. Thus, following adsorption and inhibition mechanism was proposed involving inhibitor molecules on N80 steel surface (Figure 3.2.8):

(1) Neutral N atoms in inhibitor molecules can be protonated in acid solution:



Since Cl^- ions are already adsorbed on the metal surface hence they favor more adsorption of protonated inhibitor molecules on the N80 steel surface through electrostatic interaction (physical adsorption).

(2) The protonated inhibitor molecules in acid medium start competing with H^+ ions for electrons on N80 steel surface. After the release of H_2 gas, cationic form of inhibitor molecules returns to its neutral form and the heteroatoms with free lone pair electrons promote chemical adsorption.

(3) To relieve the extra negative charge from the metal the electron from the d-orbital of Fe might be transferred to vacant π -antibonding orbital of inhibitor molecules (retro donation) and hence strengthen the adsorption.

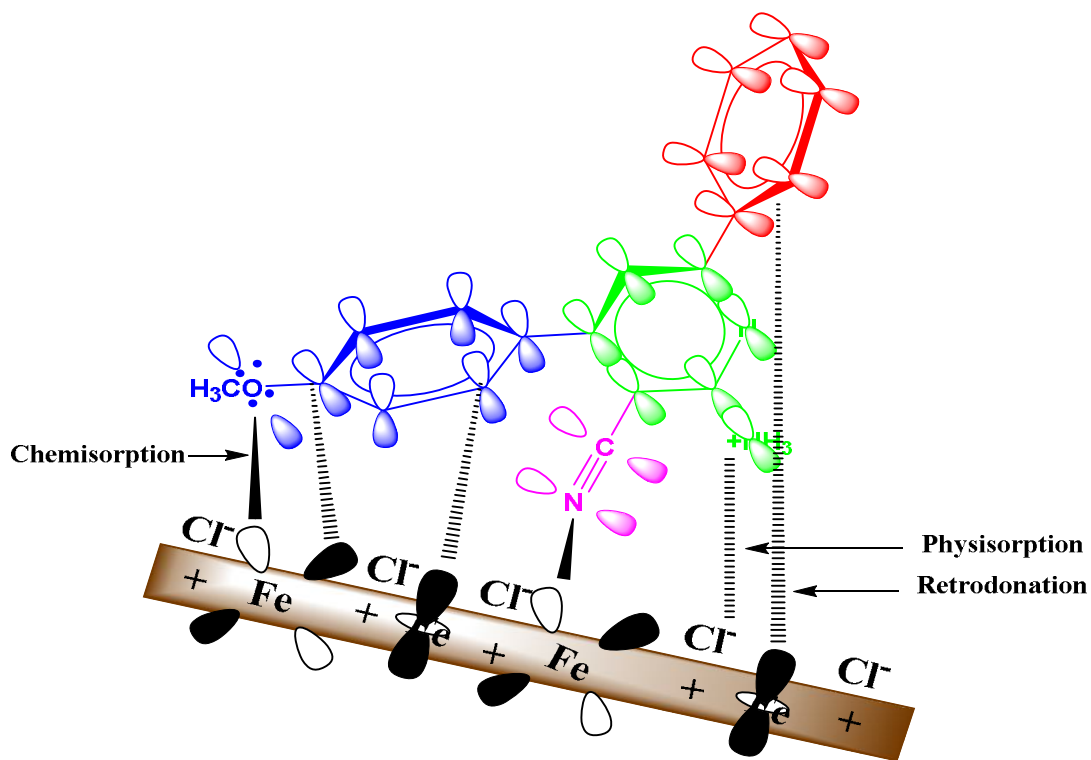


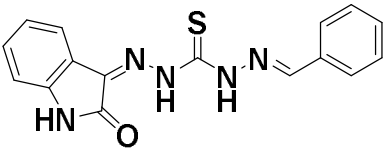
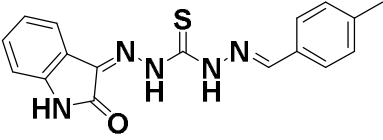
Figure 3.2.8: Plausible adsorption model of AMP on to N80 steel surface in HCl

3.3. Isatin derivatives as Corrosion Inhibitors

Isatin derivatives are important compounds which produce chemotherapeutic effects [Gangarapu *et al.* (2012), Verma *et al.* (2004), Sharaf (1997)]. Previously Yadav *et al.* have reported isatin derivatives as corrosion inhibitors in 15% HCl with the inhibition efficiency range of 91 to 84 % at 200 mgL⁻¹ [Yadav *et al.* (2013 b)], but their synthetic routes followed conventional methods which are not environmentally benign. Also literature survey reveals that little attention has been devoted for the development of corrosion inhibitors in 20% sulfuric acid [Khan and Quraishi (2010)].

Therefore, keeping an eye on the industrial and environmental scenarios, the present study deals with the synthesis of two Isatin derivatives namely 1-Benzylidene-5-(2-oxoindoline-3-ylidene) Thiocarbohydrazone (TZ-1) and 1-(4-Methylbenzylidene)-5-(2-oxoindolin-3-ylidene) Thiocarbohydrazone (TZ-2) and their application as corrosion inhibitor on mild steel in 20% H₂SO₄ medium. The inhibitive activity of TZ-1 and TZ-2 is examined successively via weight loss measurements, electrochemical impedance spectroscopy (EIS), Potentiodynamic polarization, Langmuir isotherm, scanning electron microscopy (SEM), energy-dispersive X-ray spectroscopy (EDX) and Quantum chemical methods. The molecular structure, abbreviations and IUPAC names of the synthesized compounds are given in Table 3.3.1.

Table 3.3.1 The IUPAC Name, molecular structure and abbreviation of Isatin derivatives used

| S. No. | IUPACName | Molecular Structure | Abbreviation |
|--------|--|--|--------------|
| 1 | 1-Benzylidene-5-(2-oxoindoline-3-ylidene) Thiocarbohydrazone |  | TZ-1 |
| 2 | 1-(4-Methyl benzylidene)-5-(2-oxoindolin-3-ylidene) Thiocarbohydrazone |  | TZ-2 |

3.3.1. Weight loss measurements

(i) The inhibition efficiency with different concentration of TZs was compiled in Table 3.3.2. It can be observed that gradual increase in inhibitor concentration decreases the corrosion rates (C_R) and increases the inhibition efficiency (η %). Maximum increase in inhibition efficiency (99.7%) was obtained for TZ-2 at 300 mgL⁻¹. The order of inhibition efficiencies (η %) are as follows: TZ-2 > TZ-1.

Table 3.3.2

Corrosion parameters for the mild steel in 20% H₂SO₄ containing various concentrations of TZs at 308 K obtained from weight loss measurements

| Inhibitor | Concentration (mgL ⁻¹) | C_R (mmy ⁻¹) | η (%) |
|------------------------------------|------------------------------------|----------------------------|------------|
| 20% H ₂ SO ₄ | 0.0 | 143.81 | -- |
| TZ-2 | 100 | 40.98 | 71.5 |
| | 150 | 16.50 | 88.5 |
| | 200 | 8.97 | 93.7 |
| | 250 | 3.43 | 97.6 |
| | 300 | 0.396 | 99.7 |
| TZ-1 | 100 | 48.04 | 66.5 |
| | 150 | 39.46 | 72.5 |
| | 200 | 27.98 | 80.5 |
| | 250 | 22.30 | 84.4 |
| | 300 | 15.84 | 88.98 |

(ii) The effect of temperature on the corrosion rate (C_R) of mild steel was studied in the temperature range of 308 to 328 K in 20% H₂SO₄ following an immersion period of 6h at optimum concentration (300 mgL⁻¹) of TZs and the results are shown in Figure 3.3.1.

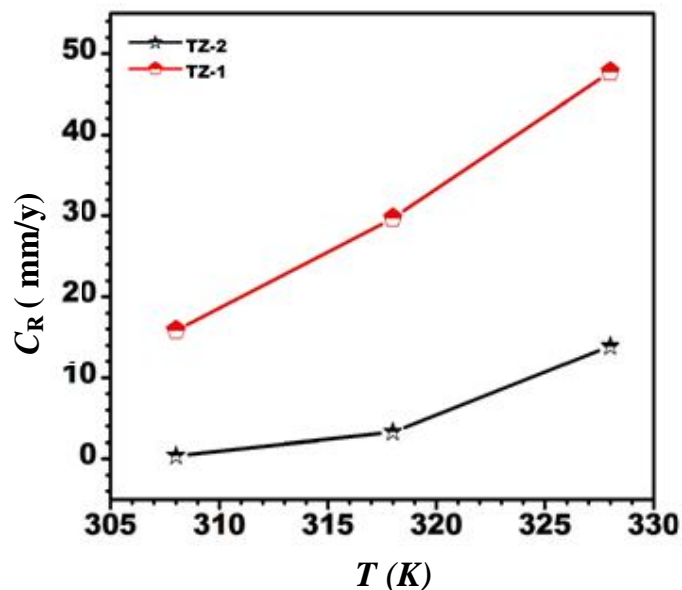


Figure 3.3.1: Variation of corrosion rate with temperature

From Figure 3.3.1, it can be observed that the corrosion rate increases as temperature increases. This increase in C_R arises due to desorption of the TZs molecules from the mild steel surface [Fouda and Ellithy (2009)].

3.2.2. Thermodynamic Parameters and Adsorption Considerations

The activation energy (E_a) for mild steel corrosion in absence and presence of the TZs was determined from the Arrhenius equation [Tao *et al.* (2009)]. Arrhenius plots of $\log C_R$ and $1/T$ are shown in Figure 3.3.2 (a). The E_a values determined from the Arrhenius plots in absence of TZs and in presence of TZ-1 and TZ-2 are tabulated in Table 3.3.3. The E_a values are lower in the absence of TZs in comparison to that in its presence. A higher value of E_a in presence of TZs indicates the physisorption as stated by others [Amar *et al.* (2007), Aljourani *et al.* (2009), Larabi *et al.* (2005)]. But Vračar, Dražić' [Vračar and Drazic (2002)] indicate that the adsorption types can't be clearly understood only by the change of activation energy because a competitive adsorption occurs with water molecules whose removal from the mild steel surface also requires some activation energy. In other sense physisorption process simultaneously may have

some chemical process and vice versa. Thus both physical and chemical processes are taking place in the adsorption of the TZs.

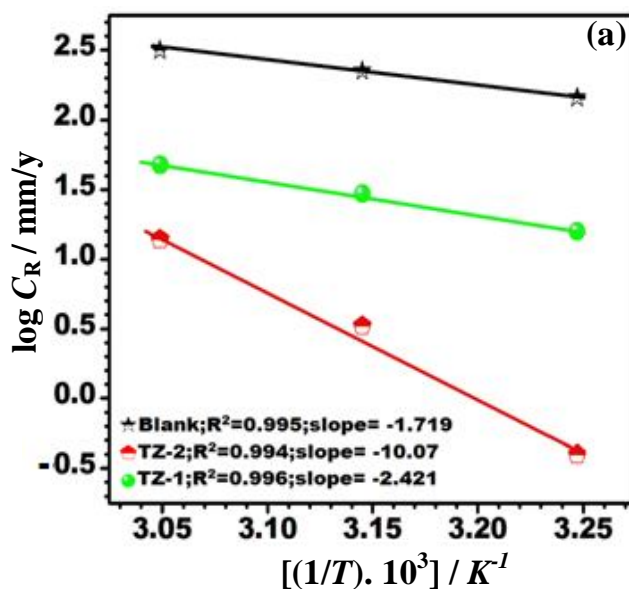


Figure 3.3.2(a): Arrhenius plots of $\log C_R$ vs. $1000/T$ in absence and presence of TZs

Table 3.3.3

Thermodynamic parameters for the adsorption of TZs on mild steel at optimum concentration in 20% H_2SO_4 at 308 K

| Inhibitors | E_a (kJ mol ⁻¹) | K_{ads} ($\times 10^3 M^{-1}$) | $-\Delta G_{ads}^\circ$ (kJ mol ⁻¹) |
|------------|----------------------------------|---------------------------------------|--|
| Blank | 32.91 | – | – |
| TZ-1 | 46.35 | 5.62 | 32.41 |
| TZ-2 | 192.82 | 6.69 | 32.85 |

Organic compounds show the inhibition property via adsorption on metal surface, and some adsorption isotherms (Frumkin, Langmuir, Temkin, Freundlich etc.) have been widely used to study the mechanism of corrosion inhibition. In this study, Langmuir adsorption isotherm which is a plot of C/θ against C was fitted and is shown in Figure 3.3.2 (b).

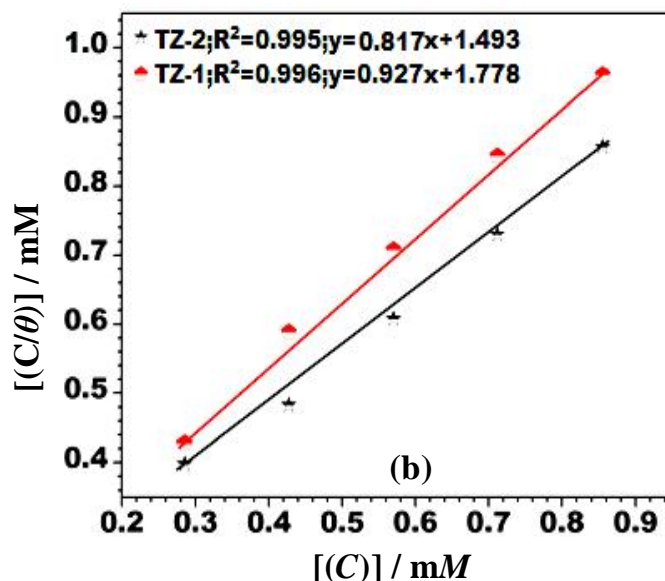


Figure 3.3.2 (b): Langmuir's isotherm plots for adsorption of TZs on mild steel surface

The correlation coefficient values for both TZs are close to 1, which indicates that the TZs adsorption on the mild steel surface is well fitted to the Langmuir adsorption isotherm.

K_{ads} can be calculated from the intercepts of the straight lines. The calculated values of K_{ads} are listed in Table 3.3.3. The values of ΔG°_{ads} in both TZs lie in the range from -20 kJ mol^{-1} to -40 kJ mol^{-1} , which probably indicates that both physisorption and chemisorption (mixed adsorption) are taking place in the system [Cano *et al.* (2004), Li *et al.* (2008)].

3.3.3. Electrochemical Impedance Spectroscopy

Electrochemical impedance spectroscopy is a commonly used technique to explain the mechanisms and adsorption phenomena in corrosion researches [Dkhireche *et al.* (2013), Danaee *et al.* (2012)]. Figure 3.3.3 (a) represents the Nyquist plots for TZs in 20% H_2SO_4 for 6 h immersion at 308 K. The impedance spectra in absence and presence of TZs exhibit a single depressed capacitive loop, which indicates that the corrosion of mild steel is mainly controlled by the charge transfer process and double layer behavior

[Behpour *et al.* (2010)]. Also the shape is maintained for both TZ-1 and TZ-2 as compared to that of the blank solution. Thus, the mechanism of the corrosion inhibition is almost the same with the addition of TZs.

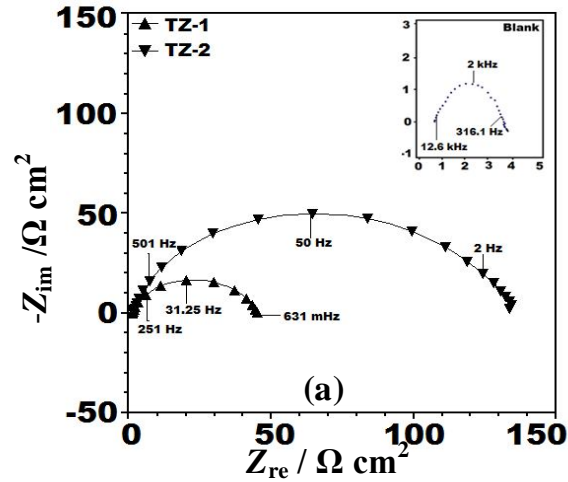


Figure 3.3.3 (a): Nyquist plots in absence and presence of optimum concentration of TZs

Bode plots in absence and presences of TZs are given in Figure. 3.3.3 (b).

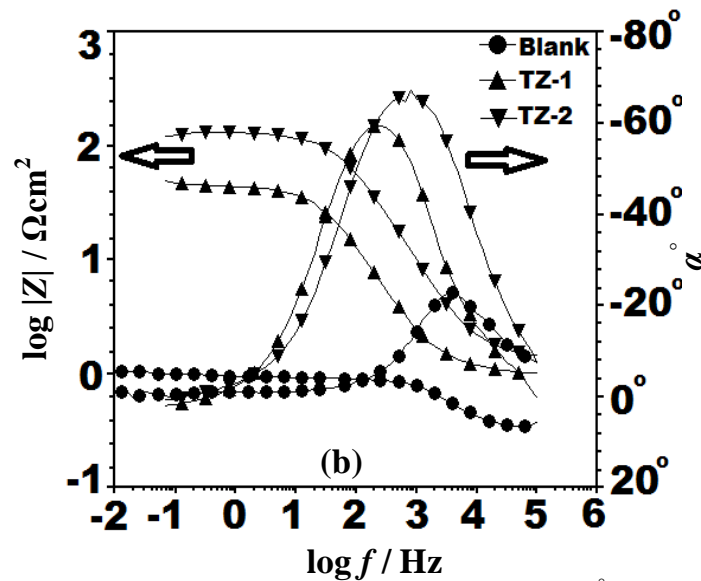


Figure 3.3.3 (b): Bode ($\log f$ vs. $\log |Z|$) and phase angle ($\log f$ vs. α°) plots in absence and

presence of optimum concentration of TZs

It can be observed from the Figure 3.3.3 (b) that the increase in low frequency impedance modulus in presence of TZ-2 is more than that in case of TZ-1. This demonstrates that the adsorption of the TZ-2 improves corrosion resistance of mild steel better than TZ-1. The values

of maxima in phase angle plots in presence of TZs approaches towards -90° (Table 3.3.4), which indicates that there is merely one time constant related to the electrical double layer formation at the electrode-solution interface [Motamedi *et al.* (2013)]. Simulation of Nyquist and Bode plots with the equivalent circuit model show excellent agreement with experimental data (Figure 3.3.3 c, d). This means that the suggested equivalent circuit model (Figure 3.3.3 e) could reasonably be used.

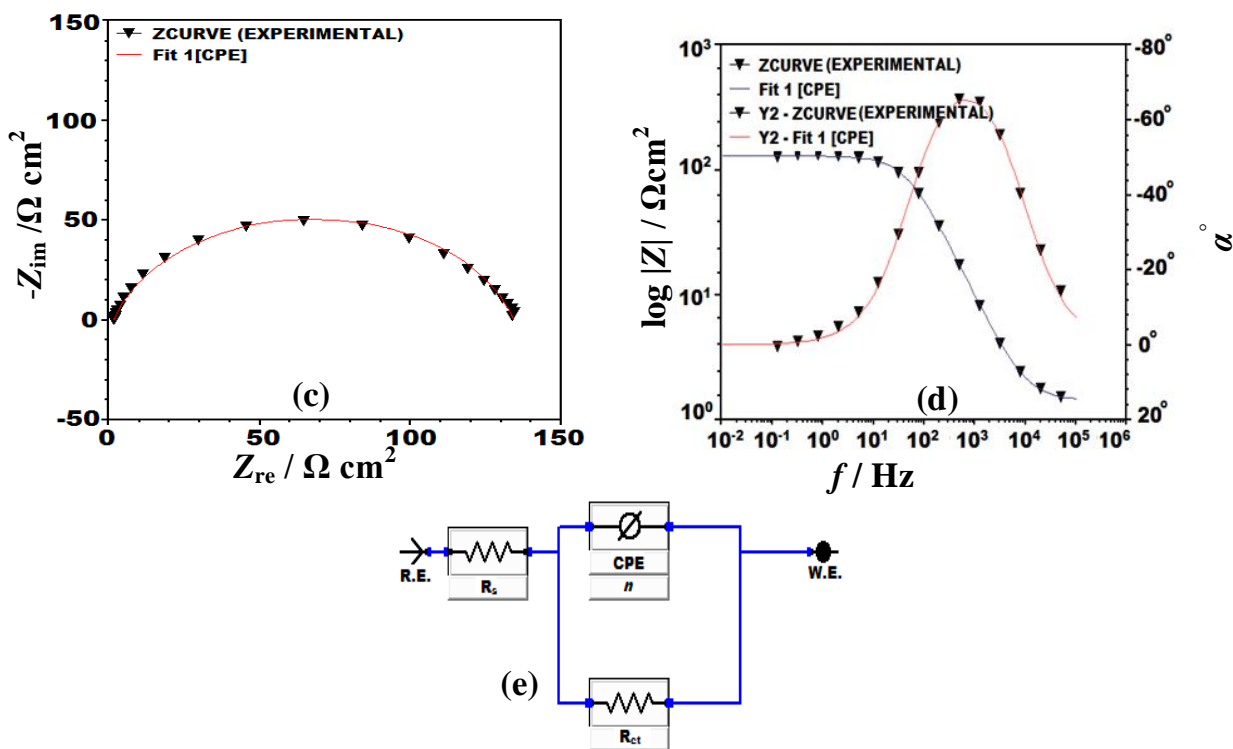


Figure 3.3.3: (c) Simulated Nyquist plot (d) Simulated Bode plot (e) Equivalent circuit

The impedance parameters obtained from the equivalent circuit are given in Table 3.3.4. A decrease in C_{dl} values in presence of the TZs as compared to that in their absence can be attributed to a decrease in the local dielectric constant and/or an increase in the thickness of the electrical double layer, which suggests that TZs molecules function by getting adsorbed at the metal/solution interface [Qu *et al.* (2007)].

Table 3.3.4

Electrochemical impedance parameters in absence and presence of optimum (300 mgL⁻¹) concentration of TZs

| Inhibitors | R_{ct} ($\Omega \text{ cm}^2$) | n | Y_0 (μFcm^{-2}) | C_{dl} ($\mu\text{F cm}^{-2}$) | η (%) | $-\alpha'$ |
|------------|---------------------------------------|-------|-----------------------------------|---------------------------------------|---------------|------------|
| Blank | 3.66 | 0.761 | 1198 | 127.9 | – | 22.6 |
| TZ-1 | 43.2 | 0.823 | 95.2 | 40.4 | 91.5 | 59.5 |
| TZ-2 | 131.3 | 0.852 | 54.3 | 23.8 | 97.2 | 67.3 |

3.3.4. Potentiodynamic polarization

Potentiodynamic polarization curves in 20% H₂SO₄ at 308 K in the absence and presence of optimum concentration (300 mgL⁻¹) of TZs are shown in Figure 3.3.4.

Different electrochemical parameters are listed in Table 3.3.5.

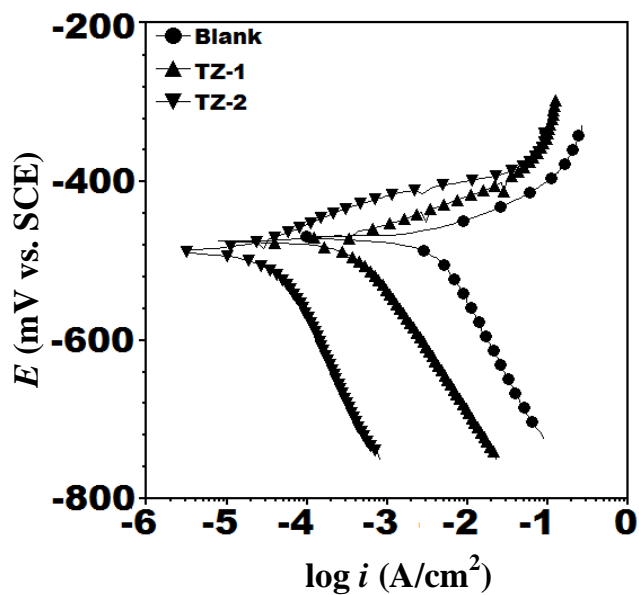


Figure 3.3.4: Potentiodynamic polarization curves for mild steel in absence and presence of optimum concentration of TZs

Table 3.3.5

Potentiodynamic polarization parameters for mild steel in absence and presence of optimum (300 mgL^{-1}) concentrations of TZs

| Inhibitor | E_{corr} (mV/SCE) | I_{corr} ($\mu\text{A}/\text{cm}^2$) | β_a (mV/dec) | β_c (mV/dec) | μ (%) |
|-----------|-------------------------------|--|-----------------------|-----------------------|--------------|
| Blank | -471 | 3410 | 52.3 | 173.9 | -- |
| TZ-1 | -475 | 405 | 43.1 | 159.8 | 88.1 |
| TZ-2 | -487 | 21.3 | 42.0 | 120.5 | 99.3 |

An assessment of Table 3.3.5 shows that there is a significant decrease in the corrosion current density after the addition of TZs, which suggests the formation of a protective film of TZs on the mild steel surface. This protective film creates a barrier between mild steel and corrosive medium during electrochemical process. Also with the addition of TZs both β_a and β_c values decreased with respect to blank. However, β_a values for both TZs do not vary significantly, while β_c values decreased slightly and this difference between TZ-1 and TZ-2 is only 31.9 mV/decade. The above discussion on the decreasing values of Tafel slopes reveals that TZs are affecting the kinetics i.e. iron dissolution and hydrogen evolution reactions. This decrease in the anodic and cathodic Tafel slopes indicates that the TZs are going to retard the anodic dissolution and hydrogen evolution reactions i.e. TZs are acting as a mixed type inhibitor by affecting both anodic and cathodic reactions. But the observation of E_{corr} values in presence of TZs reveals that there is a slight shift towards negative values i.e. cathodic site as compared to that in their absence. Thus, the above discussion shows that the studied TZs are mixed-type inhibitors but predominantly cathodic [Ansari *et al.* (2014)].

3.3.5. Surface Analysis: SEM-EDX

The formation of a protective film of the TZs on mild steel surface may be confirmed using SEM analysis. Figure 3.3.5 (a-c) represents the SEM images of mild steel in 20% H₂SO₄ in absence and presence of TZs at optimum concentration (300 mgL⁻¹) following a 6 h immersion period at 308 K. Figure 3.3.5 (a) shows that in the absence of TZs, the mild steel surface was severely damaged, whereas in the presence of both TZ-2 and TZ-1 (Figure 3.3.5 b, c), the corrosion was tangibly suppressed. This is because of the formation of a protective film of TZs on the mild steel surface. The EDX spectrum shows the absence of oxygen (O) peak in absence of TZs (Figure 3.3.5 d), which reveals that dissolution of the oxide layer. But in presence of TZs one additional peak of nitrogen (N) is observed (Figure 3.3.5 e, f), which confirms that adsorption of TZs occurs over the mild steel surface.

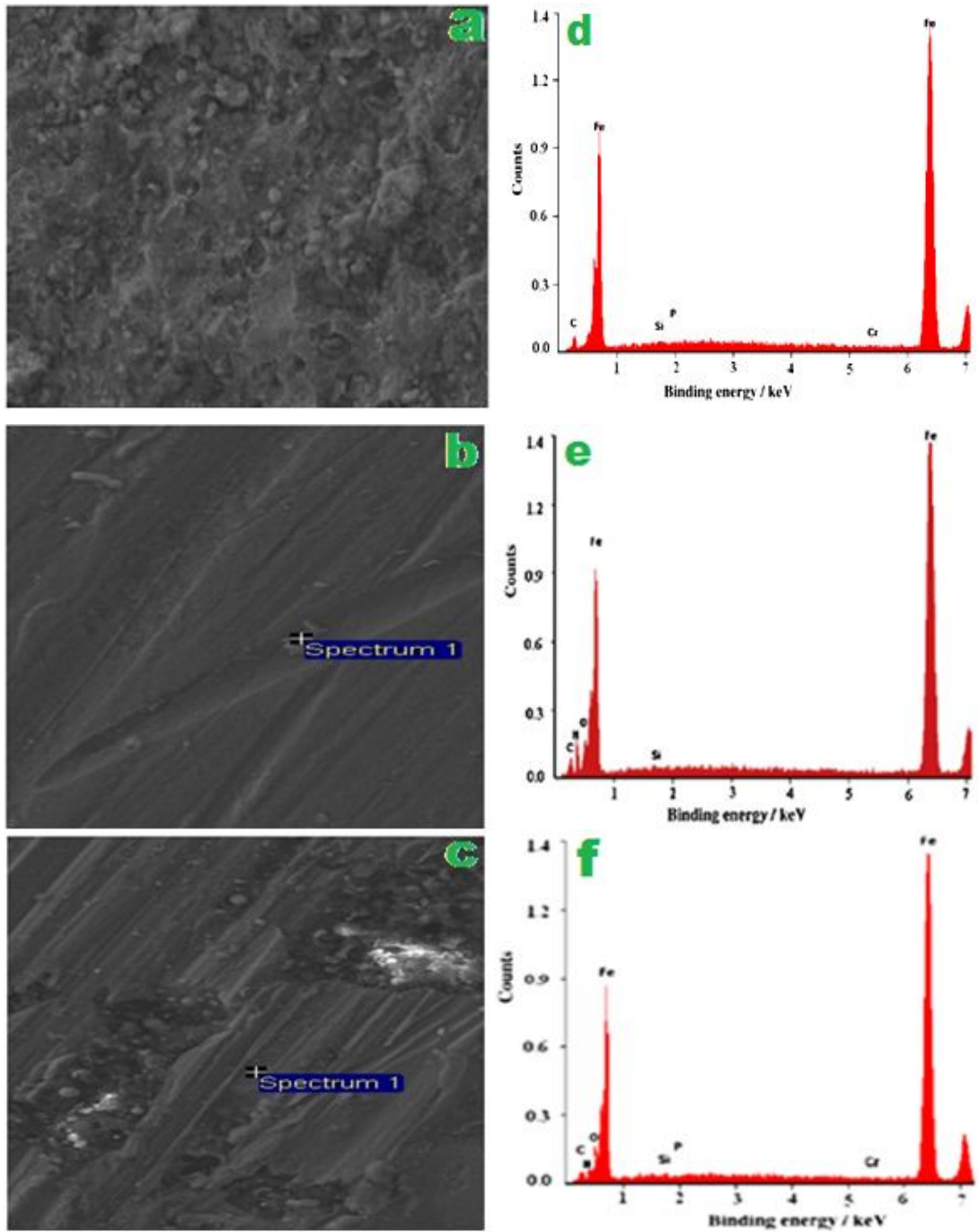


Figure 3.3.5: SEM micrographs of mild steel (a) blank 20% H₂SO₄ (b) TZ-2 (c) TZ-1
EDX micrographs of N80 steel (d) blank 20% H₂SO₄ (e) TZ-2 (f) TZ-1

3.3.6. Quantum chemical study

The optimized geometry, E_{HOMO} and E_{LUMO} of TZs both in neutral and protonated forms are shown graphically in Figures 3.3.6 (a, b), 3.3.7 (a-d) and 3.3.8 (a-d) respectively.

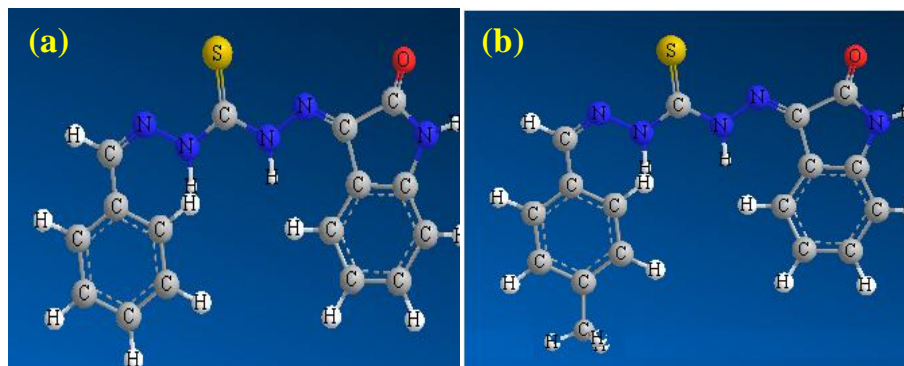


Figure 3.3.6: Optimized structures (a) TZ-1 (b) TZ-2

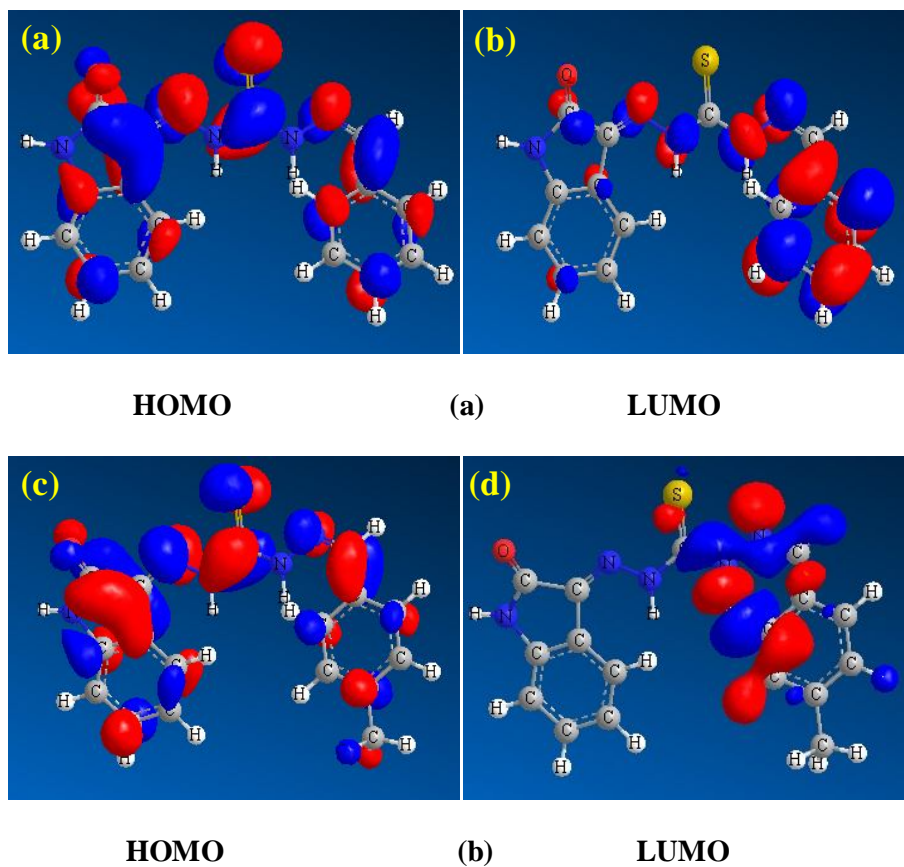


Figure 3.3.7: Frontier molecular orbitals of neutral (a) TZ-1 (b) TZ-2

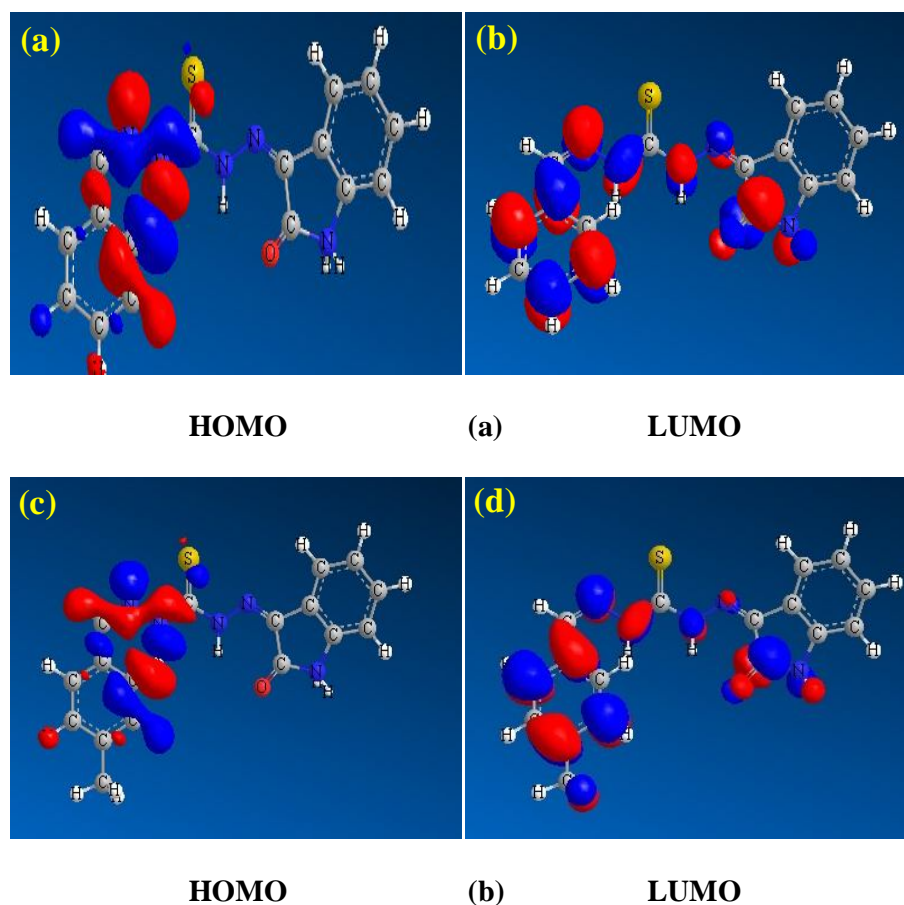


Figure 3.3.8: Frontier molecular orbitals of protonated (a) TZ-1 (b) TZ-2

As per the frontier molecular orbital theory, only frontier molecular orbitals i.e. HOMO and LUMO are involved in the course of adsorption of the inhibitor molecules [Fang and Li (2002)]. In general higher the value of HOMO, higher would be the electron donating capacity of the inhibitor to vacant d-orbital of the metal. And lower the value of LUMO, greater would be the electron accepting ability of the inhibitor from the filled metal orbitals. But the most important parameter is ΔE , which is the energy difference between LUMO and HOMO. The lower the value of ΔE easier would be the release of electron and stronger would be the adsorption [Amin *et al.* (2010)]. It is said that to become a good corrosion inhibitor, it is not only the ability to donate the electron but also to accept it in the vacant orbitals [Zhang *et al.* (2010)].

(i) Neutral TZs

The quantum data of TZs are given in Table 3.3.6.

Table 3.3.6

Calculated quantum chemical parameters of neutral and protonated inhibitors

| Inhibitors | E_{HOMO} (eV) | E_{LUMO} (eV) | ΔE (eV) |
|------------|---------------------------|---------------------------|--------------------|
| TZ-1 | -5.427 | -4.563 | 0.864 |
| TZ-2 | -5.346 | -5.022 | 0.324 |
| *TZ-1 | -9.381 | -8.655 | 0.726 |
| *TZ-2 | -9.321 | -9.089 | 0.232 |

*TZ-1 and *TZ-2 are protonated inhibitor

An inspection of Table 3.3.6 reveals that the E_{HOMO} values of TZ-2 is greater than that of TZ-1, thus TZ-2 has more electron donating capacity than TZ-1. Also E_{LUMO} value of TZ-2 is lower than TZ-1, which makes TZ-2 to accept more electrons than TZ-1 from filled d-orbitals of mild steel and causes a stronger adsorption. ΔE value of TZ-2 is lower than TZ-1, which causes TZ-2 to release electrons easily and in tern strengthens its adsorption. So, overall the adsorption order can be given as follows:

TZ-2 > TZ-1

(ii) Protonated TZs

In aqueous media there is a possibility of the inhibitor to undergo protonation. These protonated TZs then adsorb over the mild steel surface. Thus the most negative site has been protonated and their molecular properties are reported in Table 3.3.6. The ΔE values in protonated TZs are less as compared to neutral one, suggesting that protonated TZs have more reaction capacity than neutral one. So, over all in the aqueous media protonated TZs have more interaction ability than neutral one.

3.3.7. Mechanism of inhibition

The adsorption of TZs molecules on the mild steel surface can be explained by considering physisorption or chemisorption or a mixture of both processes. In the case of physisorption, TZs molecules can be adsorbed on the mild steel surface via electrostatic interaction between the charged metal surface and the protonated TZs molecules. Chemisorption of TZs molecule arises due to the donor-acceptor interaction between the lone pair of electrons present in the heteroatoms, π -electrons of multiple bonds as well as phenyl group and vacant d-orbitals of Fe [Yurt *et al.* (2004), Behpour *et al.* (2008)]. The free energies of adsorption of TZ-1 and TZ-2 are (-32.41 and -32.85 kJ mol/L respectively) which indicates that the adsorption mechanism of the TZs on mild steel surface is a mixture of both physical and chemical adsorption. Thus, adsorption of TZs can be considered to be taking place either by the cationic forms or by the neutral molecules. Therefore, the process of adsorption of TZs in case of neutral molecules occur by adsorbing onto the mild steel surface through the chemisorption mechanism, by the displacement of adsorbed water molecules from the mild steel surface and the sharing of electrons between the hetero atoms and Fe. Also, the adsorption of TZs molecules on the mild steel surface occurs via donor-acceptor interactions between π -electrons of the phenyl ring and vacant d-orbitals of Fe atoms. In the case of adsorption of protonated TZs molecules it is well known that the mild steel surface bears positive charge in acidic solution, so it is difficult for the protonated inhibitor TZs molecules to approach the positively charged mild steel surface (H_3O^+ /metal interface) due to the electrostatic repulsion. Since the SO_4^{2-} ions have a smaller degree of hydration, thus they could bring excess negative charges in the vicinity of the interface and favor more adsorption of the positively charged inhibitor molecules. The adsorption mechanism is shown in Figure 3.3.9.

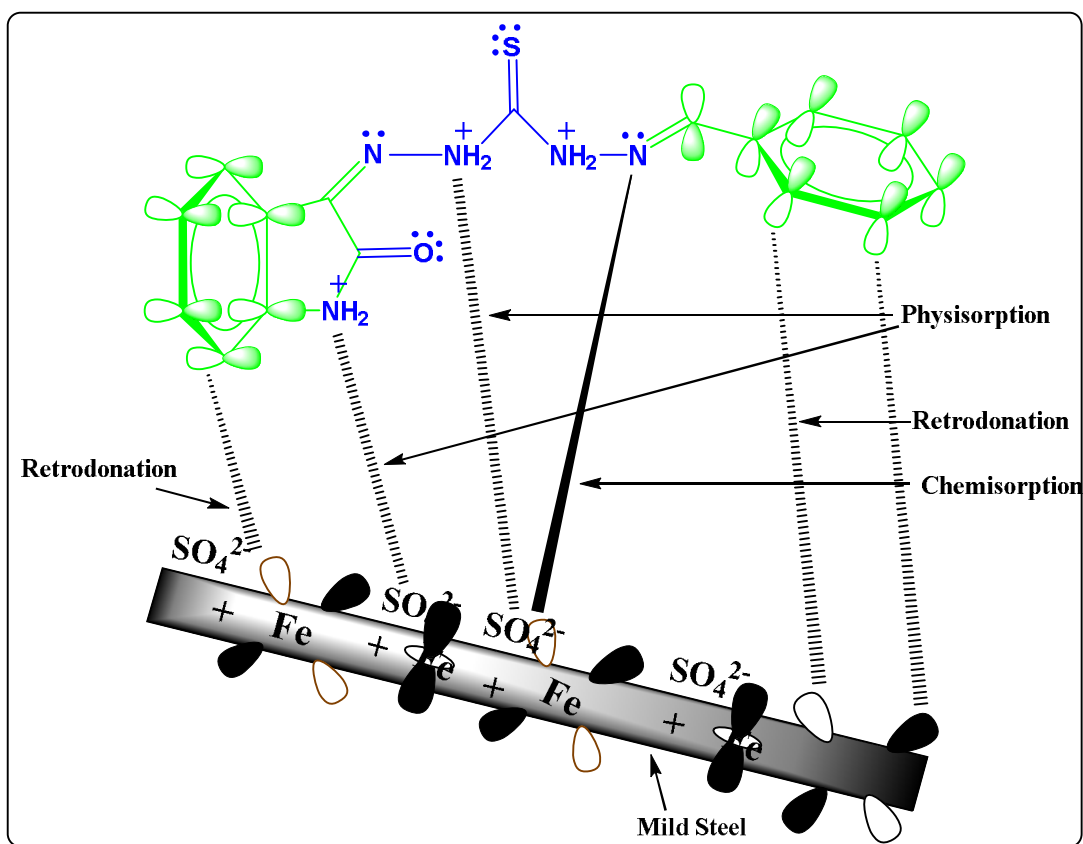


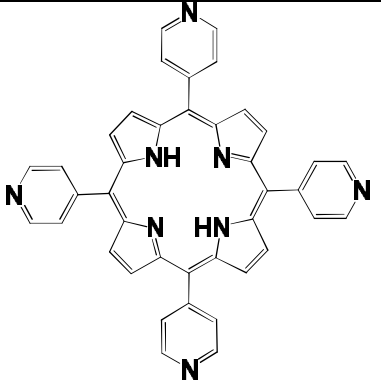
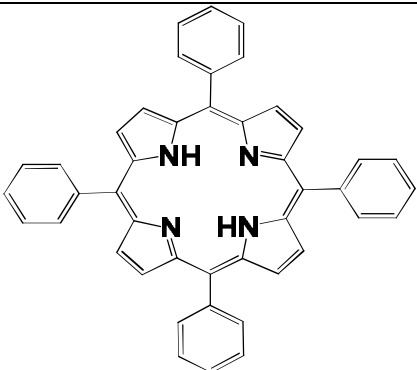
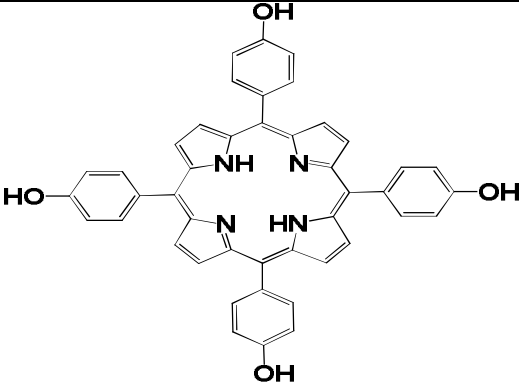
Figure 3.3.9: Plausible adsorption model of TZ-1 on to mild steel surface

3.4. Porphyrin derivatives as Corrosion Inhibitors

Porphyrins have various biological, catalytic, and photochemical properties and they are commonly used in inorganic matrices due to host guest approach. Moreover, organic- inorganic composite materials sometimes offer unique properties that are not available in any of the individual parts [Cosma *et al.* (2014)]. The porphyrin molecule is a Lewis acid with four nitrogen donor atoms at its core. It is therefore a strongly-bonding tetra-dentate chelating agent.

The aim of the present study is to investigate the corrosion inhibition property of three Porphyrins namely 5,10,15,20-Tetra (4-pyridyl) Porphyrin (P1), 5,10,15,20-Tetra phenyl Porphyrin (P2), 5,10,15,20-Tetrakis (4-hydroxyphenyl)-Porphyrin (P3) by using weight loss measurement, electrochemical impedance spectroscopy (EIS), potentiodynamic polarization, contact angle measurement, scanning electrochemical microscopy (SECM) and molecular dynamic simulation. The molecular structure, abbreviations and IUPAC name of the porphyrin derivatives are given in Table 3.4.1.

Table 3.4.1 The IUPAC Name, molecular structure and abbreviation of the Porphyrin derivatives used

| S.No. | IUPAC Name | Molecular Structure | Abbreviation |
|-------|---|--|--------------|
| 1 | 5,10,15,20-Tetra(4-pyridyl)-21H,23H-Porphyrin (P1) |  | P1 |
| 2 | 5,10,15,20-Tetraphenyl-21H,23H-Porphyrin (P2) |  | P2 |
| 3 | 5,10,15,20-Tetrakis(4-hydroxyphenyl)-21H,23H-Porphyrin(P3), |  | P3 |

3.4.1. Weight loss measurements

(i) The inhibition effect of Porphyrin derivatives at different concentrations on J55 steel corrosion in 3.5% NaCl saturated with CO₂ was studied at 308 K after 3h immersion. The relationship between inhibition efficiency (η %) and Porphyrin concentration is shown in Figure 3.4.1. The η % increases with increase in Porphyrin concentration, which is due to the adsorption of the Porphyrin molecules over J55 steel surface. The highest inhibition efficiency of 95% is shown by P1 inhibitor at 400 mgL⁻¹. The order of inhibition efficiencies is as follows: P1> P3> P2.

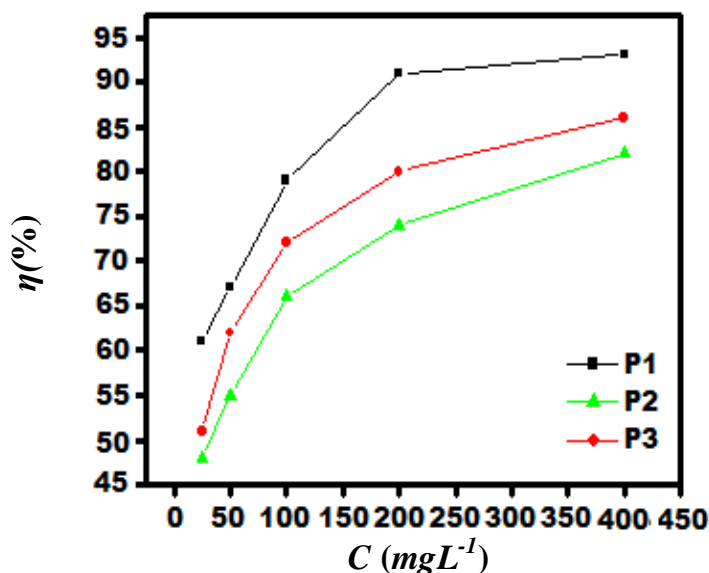


Figure 3.4.1: Variation of percentage inhibition efficiency with inhibitor concentration

3.4.2. Electrochemical Impedance Spectroscopy

The impedance spectra of J55 steel in 3.5% NaCl solution saturated with CO₂ in absence and presence of optimum concentrations (400 mgL⁻¹) of Porphyrins are presented in Figure 3.4.2 (a).

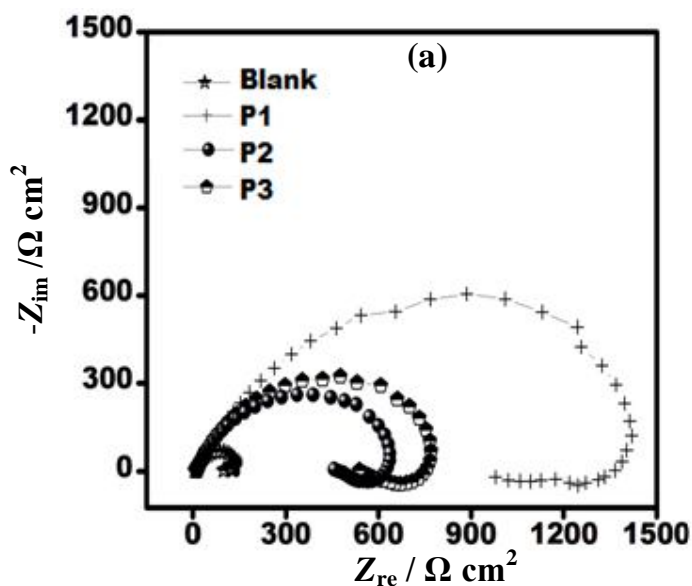


Figure 3.4.2 (a): Nyquist plots in absence and presence of optimum concentration of porphyrins

The Nyquist plots show a depressed semicircle with the center below the real axis. This behavior is typical for solid metal electrodes that show frequency dispersion of the impedance data [Ghada *et al.* (2013), Singh *et al.* (2014 a)]. The diameter of the Nyquist plot containing Porphyrins are larger than that in the blank solution, which means that the addition of Porphyrins improves the corrosion resistance of the J55 steel. The addition of Porphyrins does not change the shapes of the Nyquist plots. However, the diameter of the capacitive loop gradually increases with the addition of inhibitor, indicating the adsorption of inhibitor molecules exhibiting a barrier effect that would effectively protect the metal from aggressive attack by the solution [Doner and Kardas (2011), Solmaz *et al.* (2011), Yildiz (2015)]. The presence of inductive loop is associated with the adsorbed intermediate product [Zhang and Cheng (2009)].

Equivalent circuit [Figure 3.4.2 (b)] consisting of parallel combination of a capacitor (C_{dl}), a charge transfer resistor (R_{ct}), in series, with inductance (L), a resistor (R_s) representing the solution resistance, and CPE is used to fit the Nyquist plots.

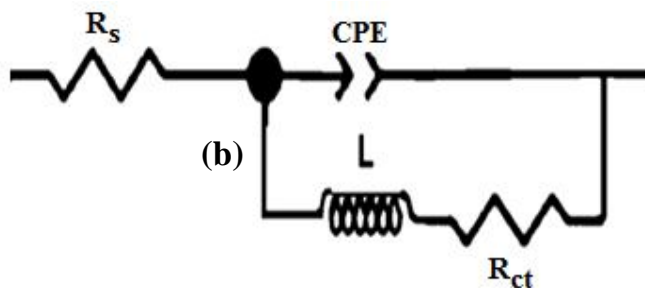


Figure 3.4.2 (b): Equivalent circuit used to fit the EIS data

From Table 3.4.2, it could be observed that the value of R_{ct} increased in presence of inhibitors, which is due to the adsorption of porphyrins molecule at the metal/solution interface [Popova *et al.* (2003)]. The better efficiency of the P1 inhibitor could be attributed due the presence of N heteroatoms in its outer moiety which could easily take part in bonding with the metal surface and thereby mitigate the corrosion effectively.

Table 3.4.2

Electrochemical impedance parameters in the absence and presence of optimum concentration (400 mgL^{-1})

| Inhibitors | R_{ct} ($\Omega \text{ cm}^2$) | n | Y_0 ($\mu\text{F cm}^{-2}$) | L (Hcm^2) | C_{dl} (μFcm^{-2}) | η (%) |
|------------|---------------------------------------|-------|------------------------------------|---------------------------|--------------------------------------|---------------|
| Blank | 119 | 0.695 | 233 | 56 | 38.01 | -- |
| P1 | 1412 | 0.808 | 99 | 22 | 31.46 | 92 |
| P2 | 656 | 0.731 | 119 | 31 | 35.56 | 82 |
| P3 | 765 | 0.748 | 102 | 28 | 32.31 | 84 |

Bode plots in absence and presence of Porphyrins is given in Figure 3.4.2 (c). The increase in low frequency impedance modulus in presence of P1 is more than that in comparison to P2 and P3 solution. This demonstrates that the adsorption of the P1 improves corrosion resistance of J55 steel better than P2 and P3 and also the low frequency impedance modulus in the presence of Porphyrins is greater than in their absence.

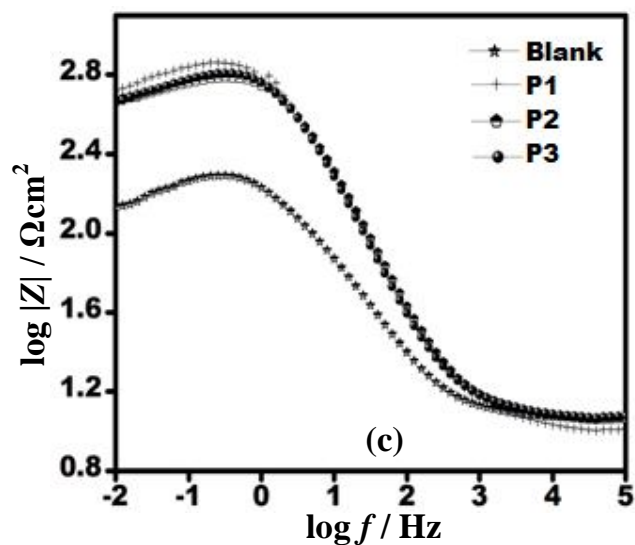


Figure 3.4.2(c): Bode ($\log f$ vs. $\log |Z|$) plots in absence and presence of optimum concentration of Porphyrins

The phase angle plots are shown in Figure 3.4.2 (d).

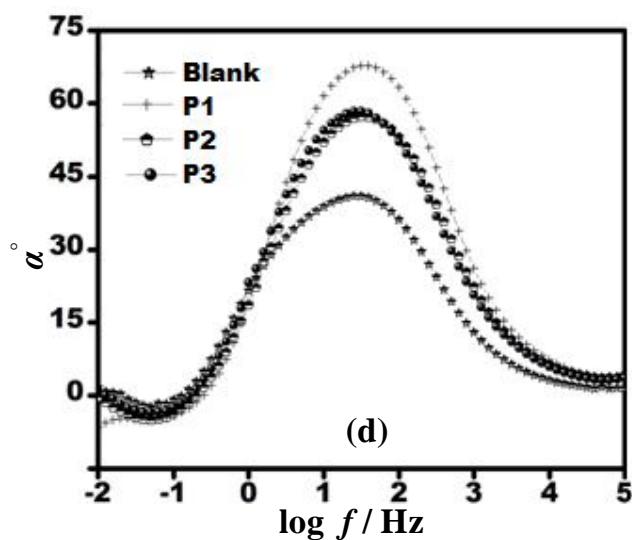


Figure 3.4.2(d): Phase angle ($\log f$ vs. α°) plots in absence and presence of optimum concentration of Porphyrins

In the intermediate frequency maximum phase angle peak and slope values in presence of Porphyrins approaches towards -90° and -1 respectively (Table 3.4.3), which is related to the electrical double layer formation at the electrode/solution interface [Lin *et al.* (2015 a), Tang *et al.* (2013)].

Table 3.4.3

The slopes of Bode impedance magnitude plots at intermediate frequencies (S) and the maximum phase angles (α°) for J55 steel in CO₂ saturated 3.5% NaCl solution in absence and presence of optimum concentration (400 mgL⁻¹) of Porphyrins

| Inhibitors | - S | $-\alpha^\circ$ |
|------------|-------|-----------------|
| Blank | 0.491 | 32.7 |
| P1 | 0.745 | 68.9 |
| P2 | 0.661 | 58.6 |
| P3 | 0.674 | 59.7 |

3.4.3. Potentiodynamic polarization

Potentiodynamic polarization curves are shown in Figure 3.4.3 for J55 steel in 3.5% NaCl solution saturated with CO₂ at 308 K in absence and presence of optimum concentrations of Porphyrins.

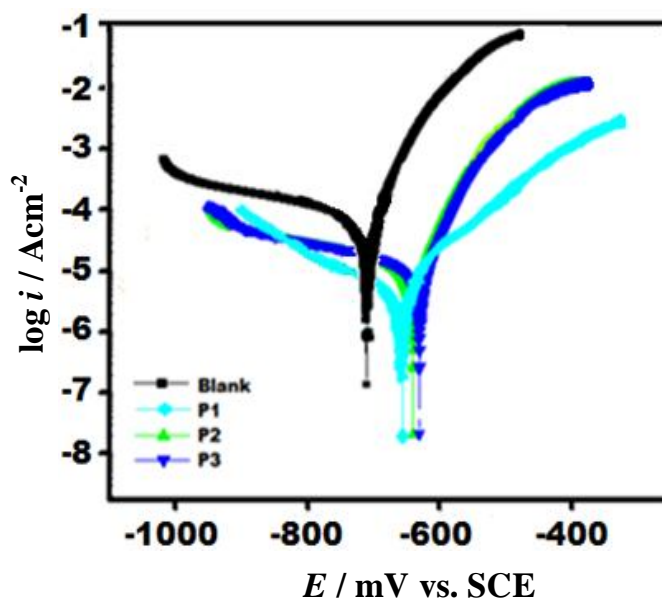


Figure 3.4.3: Potentiodynamic polarization curves in absence and presence of optimum concentration of Porphyrins

The electrochemical parameters are given in Table 3.4.4.

Table 3.4.4

Potentiodynamic polarization parameters in the absence and presence of optimum concentration (400 mgL⁻¹) of Porphyrins

| Inhibitor | E_{corr} (mV/SCE) | I_{corr} (mA/cm ²) | β_a (mV/dec) | β_c (mV/dec) | η (%) |
|------------------|-------------------------------|--|-----------------------|-----------------------|---------------|
| Blank | -721 | 0.91 | 46 | 103 | -- |
| P1 | -671 | 0.05 | 66 | 92 | 94.5 |
| P2 | -649 | 0.14 | 64 | 97 | 84.6 |
| P3 | -643 | 0.09 | 57 | 93 | 90.0 |

The analysis of Figure 3.4.3 shows that both the cathodic and anodic curves are shifted towards lower current density, which indicates the mixed mode of Porphyrins action i.e. acting on both the hydrogen evolution reaction and metal dissolution. The value of I_{corr} decreases with the addition of Porphyrins. The values of β_c are almost constant but that of β_a changed significantly. The shifts in corrosion potential (E_{corr}) values in presence of Porphyrins occurs towards positive or anodic direction. Thus, the inhibitor is mixed type but predominantly anodic.

3.4.4. Adsorption characteristics of the inhibitor

The values of surface coverage (θ) from weight loss experiments at different concentrations (C) of Porphyrins were tested graphically for fitting of a suitable adsorption isotherm [Yadav *et al.* (2012 b), Naderi *et al.* (2009)]. A graph between C/θ versus C , (Figure 3.4.4) showed a linear fit suggesting the adsorption of Porphyrins on the metal surface obeyed Langmuir adsorption isotherm. The plots of all the Porphyrins were close to unity [Singh *et al.* (2014 b), Lebrini *et al.* (2007)].

The calculated values of $\Delta G_{\text{ads}}^{\circ}$ for Porphyrins are -35.6 kJ mol⁻¹ (P1), -34.5 kJ mol⁻¹ (P2), and -34.2 kJ mol⁻¹ (P3), which probably means that both physical adsorption and chemical adsorption (comprehensive adsorption) would take place [Singh *et al.* (2014 b), Xomet *et al.* (2008)].

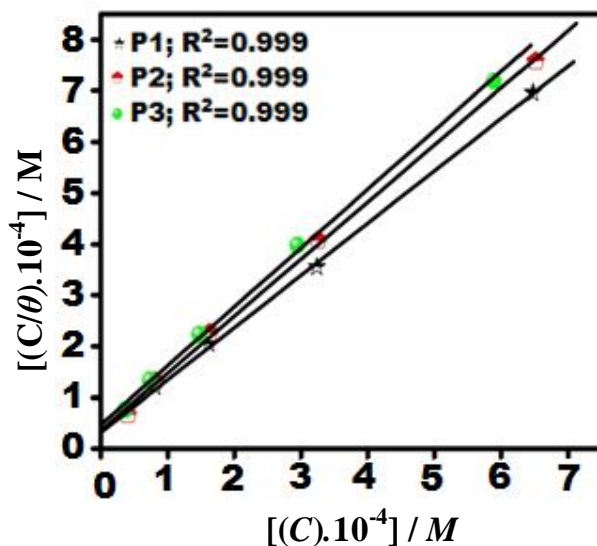


Figure 3.4.4: Langmuir's isotherm plots in absence and presence of optimum concentration of Porphyrins

3.4.5. Contact Angle measurement

The contact angle measurements were carried out at 308 K. A base line test without corrosion inhibitor was carried out first after which the corrosion inhibitors were injected on the J55 steel surface. Droplets were placed on the steel surface by a syringe. For each concentration of corrosion inhibitor the contact angle measurements were repeated 3 times [Lin *et al.* (2015 b)]. The syringe used was cleaned with acetone each time before the tests. The contact angle in absence of inhibitor was 14.7° meaning that the surface behaved as hydrophilic (having strong affinity for water). The contact angle increased with the addition of Porphyrins and the steel surface became hydrophobic (lacking affinity for water). At high concentration of the Porphyrins, the droplet formed a very small contact angle as is evident from Figure 3.4.5. All the Porphyrins showed hydrophobic nature but P1 inhibitor showed the best result with an angle of 112.4°. These results confirm the formation of hydrophobic layer on the J55 steel surface in presence of Porphyrins.

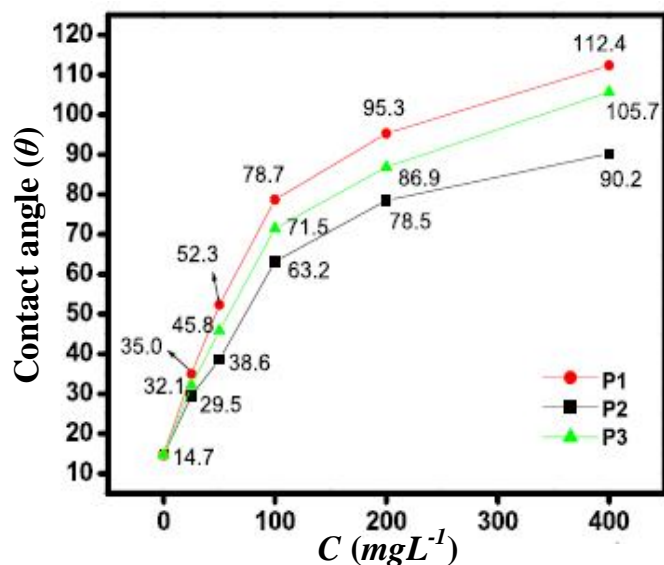
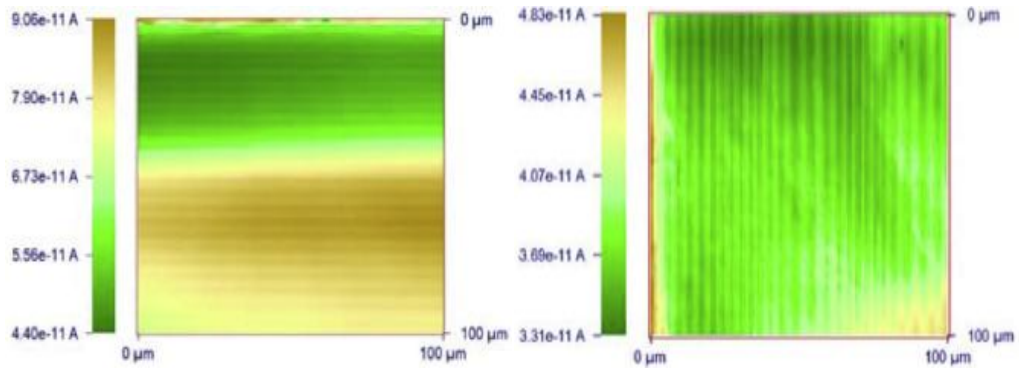


Figure 3.4.5: Contact Angle versus concentration plots for Porphyrins

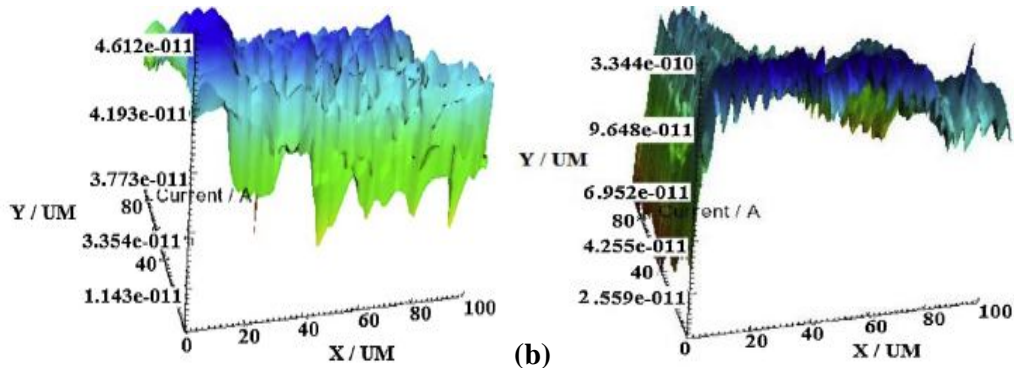
3.4.6. Scanning Electrochemical Microscopy (SECM)

Figure 3.4.6 shows the SECM images in the form of color mapping and 3D figures. Figure 3.4.6 (a-h) shows the x-axis and y-axis images of the metal surface as visualized by scanning electrochemical microscope. A probe approach curve test was performed on both x-axis and y-axis to confirm that the tip was in the vicinity of the metal surface [Singh *et al.* (2015 a), Singh *et al.* (2014 c), Liu *et al.* (2014)]. The color mapping figure for blank showed variations in color due to rapid change in the current, when the tip was in close proximity to the metal surface [Figure 3.4.6 (a)]. The color changed slightly in the presence of Porphyrins on both x and y axes as shown in Figure 3.4.6 (c, e and g). The color mapping figures suggest that the surface is less corroded in the presence of Porphyrins while rough in its absence. A lower current is observed when the tip of the probe is brought near the metal surface with Porphyrins (insulating surface). This may be ascribed to the insulating film that blocks the diffusion of mediator toward the tip as shown in Figure 3.4.6 (d, f and h) [Singh *et al.* (2014 d)]. On the other hand, the current increases when the tip of the probe is brought near the metal surface without inhibitor (conducting surface). This may be accounted to the presence of redox mediator

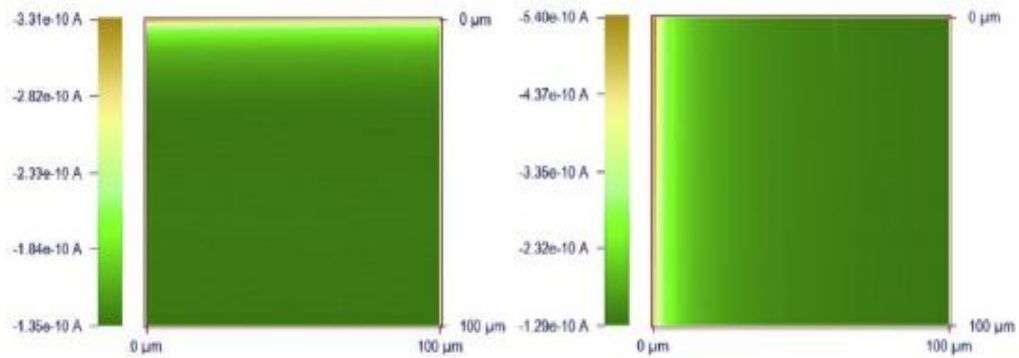
that revived at the surface as shown in Figure 3.4.6 (b) [García *et al.* (2010)]. The J55 steel surface devoid of Porphyrins remains conductive, and insulating in presence of inhibitors, that can be confirmed by an enhancement in the current (conducting) and by a reduction in the current (insulating) [Maljusch, *et al.* (2012)].



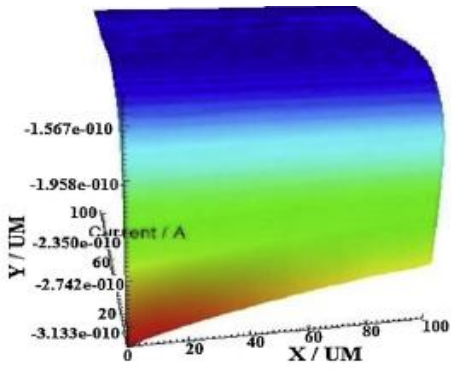
(a)



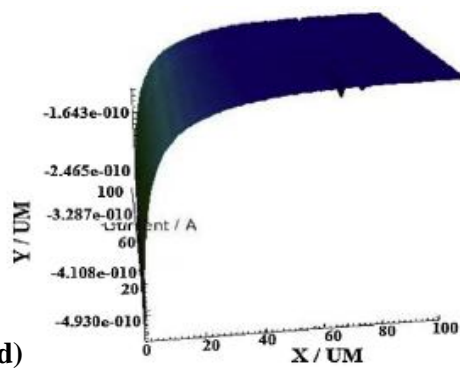
(b)



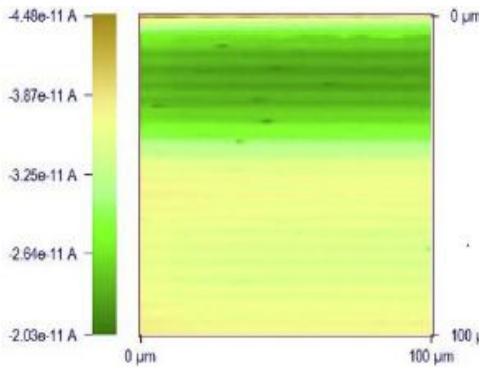
(c)



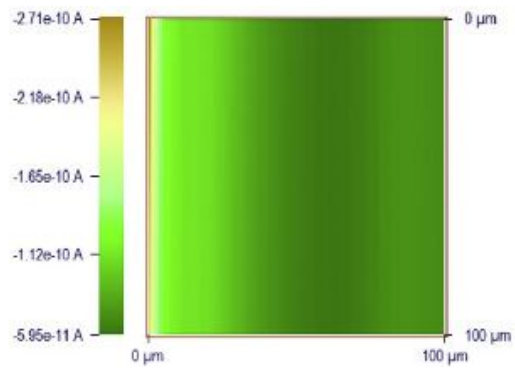
(d)



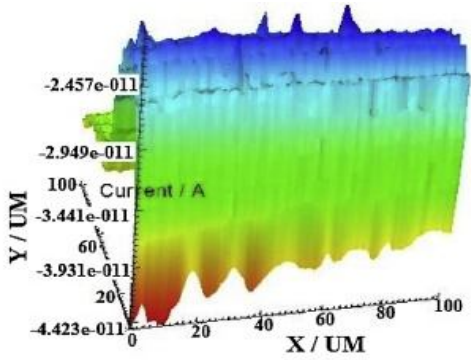
(e)



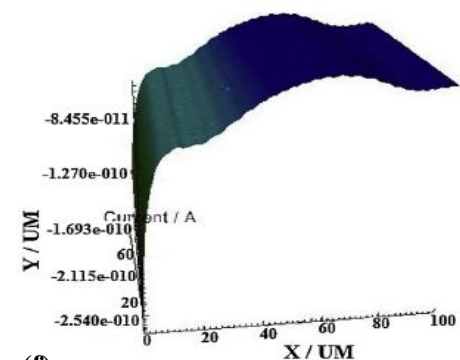
(f)



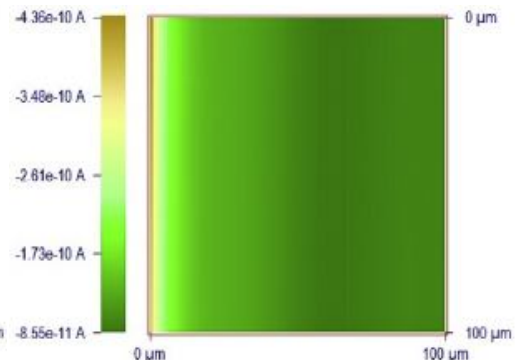
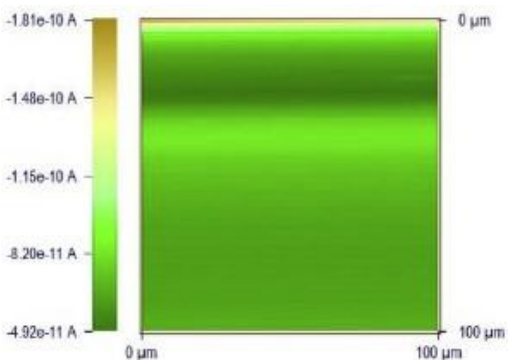
(g)



(h)



(i)



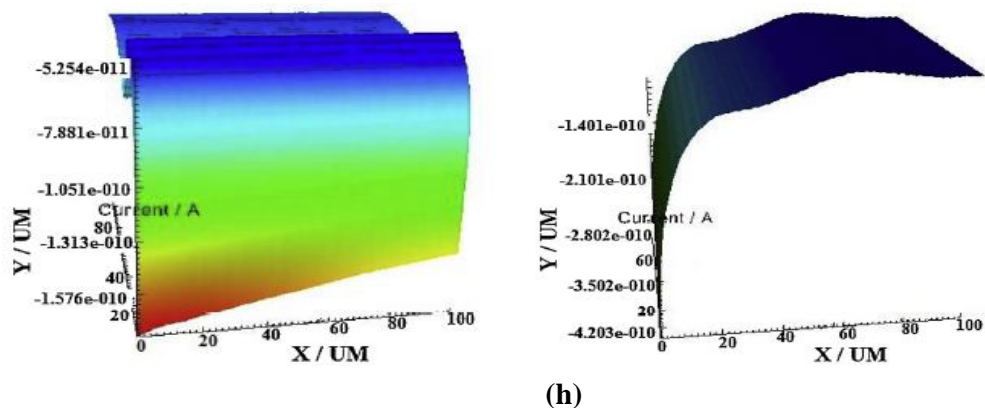
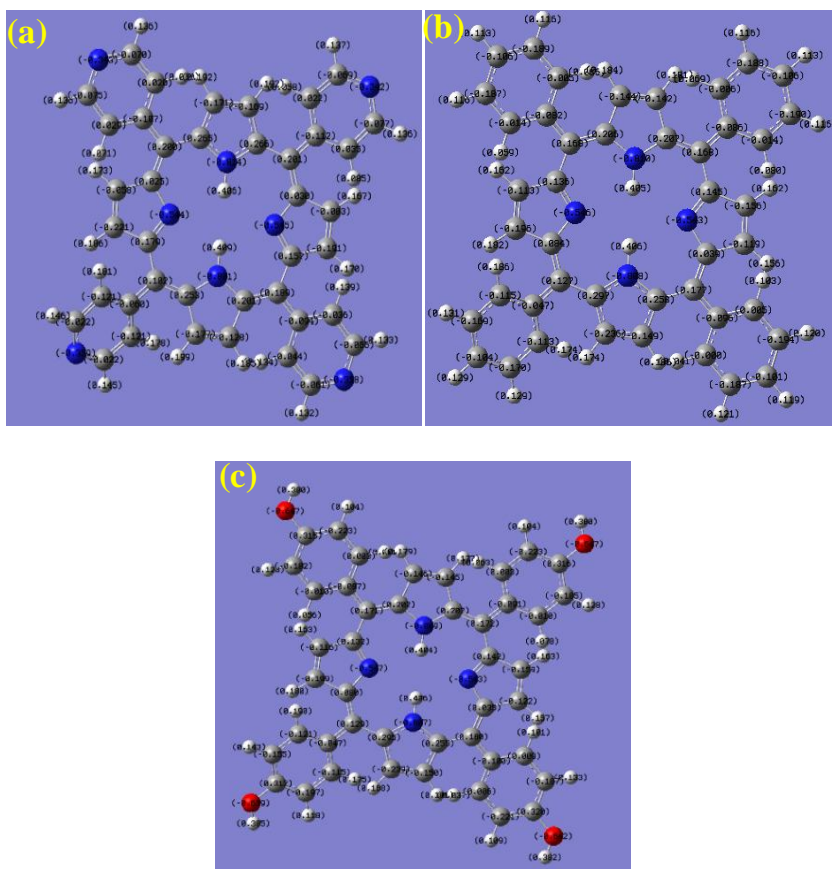


Figure 3.4.6: SECM (a) 3.5% NaCl x and y axis (b) 3.5% NaCl x and y axis 3D (c) P1 x and y axis (d) P1 x and y axis 3D (e) P2 x and y axis (f) P2 x and y axis 3D (g) P3 x and y axis (h) P3 x and y axis 3D

3.4.7. Quantum chemical study

Neutral inhibitors: The optimized geometries (with Mulliken charges), HOMO and LUMO distributions of P1, P2 and P3 are shown in Figure 3.4.7 (a-i).



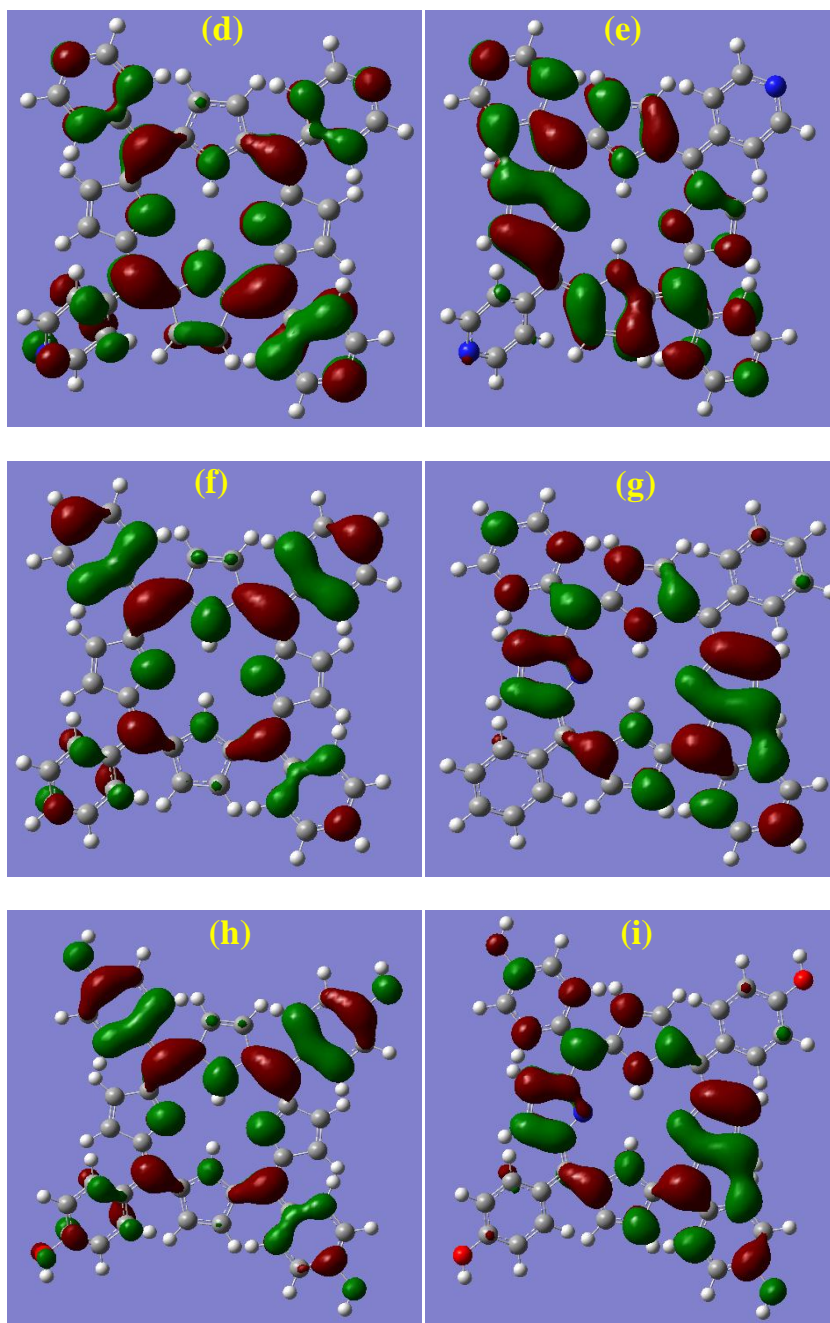


Figure 3.4.7: Optimized geometries of neutral inhibitors (a) P1 (b) P2 (c) P3, Frontier molecular orbital's of neutral P1 (d) HOMO (e) LUMO, P2 (f) HOMO (g) LUMO and P3 (h) HOMO (i) LUMO

Neutral inhibitors: All quantum chemical parameters are given in Table 3.4.5 for neutral forms of inhibitors. It is reported in the literature that interaction between the reactants takes place via the involvement of frontier molecular orbital's i.e. HOMO and LUMO. HOMO energy is associated with electron donation ability of the inhibitor. So, higher the

HOMO energy, more easily the electrons can be donated by the inhibitor to the unoccupied d-orbital's of the metal. However LUMO energy is associated with the electron acceptance tendency of the molecule. Thus, lower the LUMO energy; more easily inhibitor molecule can accept electrons from the filled metal orbitals. Consequently, the value of the energy gap $\Delta E = E_{LUMO} - E_{HOMO}$, represents the reaction tendency of the inhibitor i.e. lower its value, higher would be the inhibition efficiency.

Table 3.4.5

Calculated quantum chemical parameters of neutral and protonated inhibitors

| Inhibitors | E_{HOMO} (eV) | E_{LUMO} (eV) | ΔE (eV) |
|------------|--------------------|--------------------|--------------------|
| P1 | -4.188 | -3.563 | 0.625 |
| P2 | -5.494 | -2.671 | 2.823 |
| P3 | -4.575 | -2.885 | 1.690 |
| *P1 | -6.990 | -3.769 | 3.221 |
| *P2 | -7.697 | -2.736 | 4.961 |
| *P3 | -7.352 | -2.989 | 4.363 |

*P1,*P2 and *P3 are protonated inhibitor

The value of E_{HOMO} is higher in the case of P1 than P2 and P3, which is due to the presence of electron donor pyridyl substituent in the molecular framework of P1. So, P1 has higher electron donating ability. The ΔE value of P1 is lower as compared to P2 and P3, which further supports its more inclination to adsorb. This is in good agreement with the experimentally observed result i.e. P1 is better inhibitor than P2 and P3.

Protonated inhibitors: In aqueous system inhibitor molecules have the tendency to undergo protonation by using their lone pairs of electrons. It has been reported that these protonated species can also take part in adsorption process. So, it becomes necessary to explain the adsorption of these protonated species. The site which has most negative Mulliken charge would undergo protonation and there corresponding quantum chemical parameters are given in Table 3.4.5. After comparing the ΔE values of neutral and

protonated inhibitors (Tables 3.4.5), it could be said that the values of ΔE in all inhibitors are lower in neutral forms than protonated forms, which reveals that neutral species are more reactive than protonated species i.e. greater tendency to interact with the metal. Thus, neutral forms of inhibitors are more likely to get adsorbed on the J55 steel surface than protonated forms.

3.4.8. Molecular dynamic simulations

Figure 3.4.8 (a-c) represents Molecular dynamic simulations for the adsorption of porphyrins on J55 steel surface.

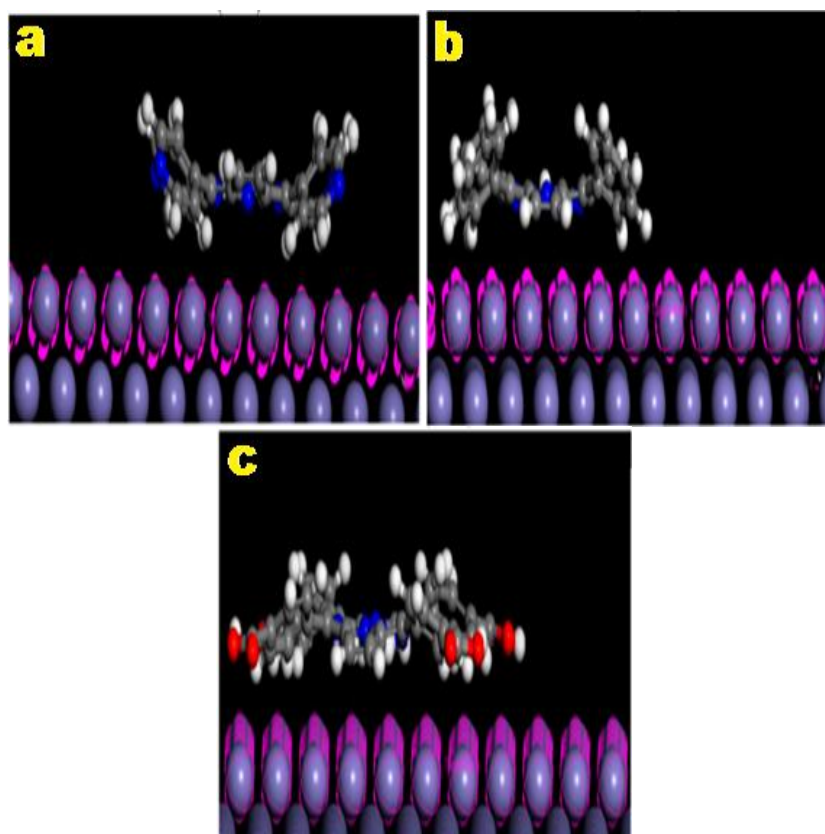


Figure 3.4.8: Molecular dynamic simulations (a) P1 (b) P2 (c) P3

It is documented in the literature that more negative is adsorption energy stronger will be the adsorption of the inhibitor [Kabanda *et al.* (2013)]. The adsorption energies of P1, P2 and P3 are -368.11 kcal/mol, -274.10 kcal/mol and -276.84 kcal/mol respectively. Thus,

P1 has most negative adsorption energy, which reveals its greater adsorption than P2 and P3. So, this study also supports the experimentally observed results.

3.4.9. Mechanism of corrosion mitigation

When CO₂ gas is passed in NaCl solution, it reacts with water molecules and forms carbonic acid. In this acidic solution, steel surface becomes positively charged (Figure 3.4.9). So, initially Cl⁻ ions may get adsorbed on positively charged J55 steel surface. This acidic environment causes protonation of inhibitor molecules. This protonated inhibitor then interacts with the Cl⁻ and gets adsorbed through electrostatic interactions (physical adsorption), by forming a protective layer (FeCl-inhibitor⁺)_{ads} [Singh *et al.* (2015 b)]. Also the inhibitor molecule contains lone pair of electrons on heteroatoms which are donated to vacant 3d-orbitals of iron atoms (chemical adsorption). In order to make a strong adsorption layer, filled orbitals of iron atoms give their electrons to the vacant orbital of inhibitor molecules via retro-donation.

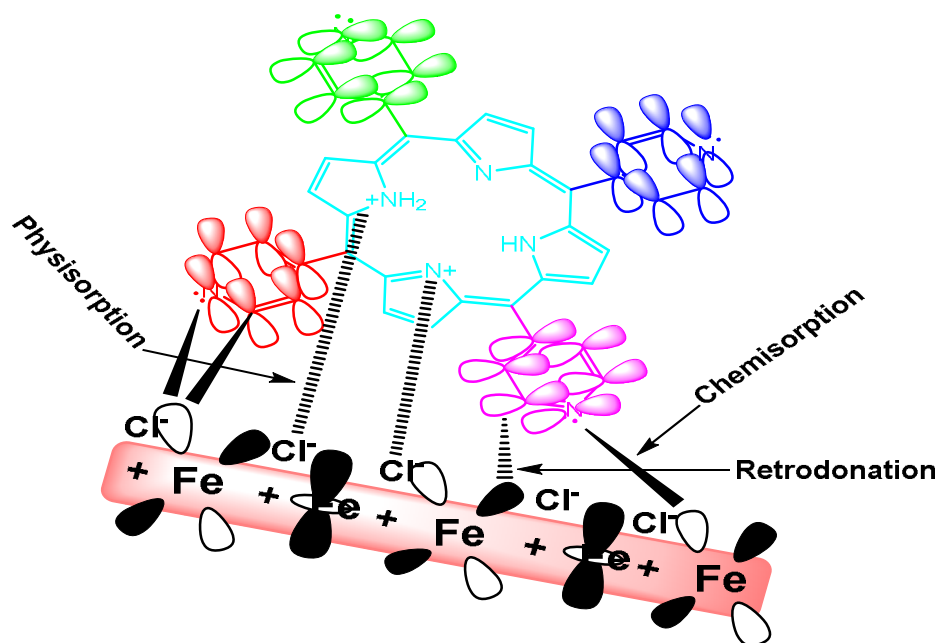


Figure 3.4.9: Mechanism of corrosion mitigation of P1 in 3.5% NaCl solution saturated with CO₂